
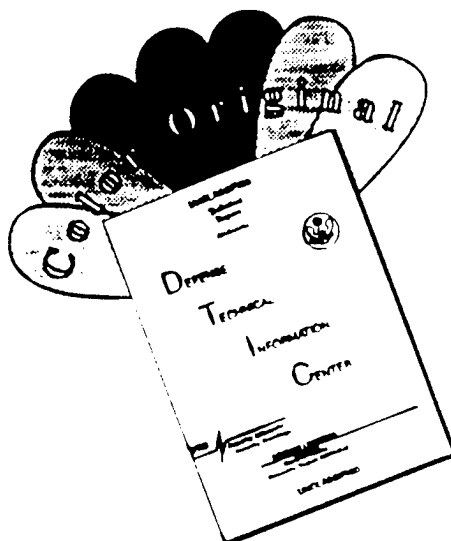


LOAN DOCUMENT

DTIC ACCESSION NUMBER	PHOTOGRAPH THIS SHEET	INVENTORY																		
																				
	LEVEL																			
<p><u>Lateral Jet Effectiveness Studies...</u></p> <p>DOCUMENT IDENTIFICATION Sep 96</p>																				
<div style="border: 1px solid black; padding: 5px; margin: 0 auto; width: 80%;"> <p>DISTRIBUTION STATEMENT A</p> <p>Approved for public release Distribution Unlimited</p> </div>																				
DISTRIBUTION STATEMENT																				
<p>ACCESSION FOR</p> <table style="width: 100%; border-collapse: collapse;"> <tr> <td style="width: 50%;">NTIS</td> <td style="width: 50%;">GRAM</td> <td style="width: 50%; text-align: center;"><input checked="" type="checkbox"/></td> </tr> <tr> <td>DTIC</td> <td>TRAC</td> <td style="text-align: center;"><input checked="" type="checkbox"/></td> </tr> <tr> <td>UNANNOUNCED</td> <td></td> <td style="text-align: center;"><input type="checkbox"/></td> </tr> <tr> <td colspan="3">JUSTIFICATION</td> </tr> </table> <p>BY _____</p> <p>DISTRIBUTION/ _____</p> <p>AVAILABILITY CODES</p> <table style="width: 100%; border-collapse: collapse;"> <tr> <td style="width: 33%;">DISTRIBUTION</td> <td style="width: 33%;">AVAILABILITY AND/OR SPECIAL</td> <td style="width: 33%;"></td> </tr> <tr> <td style="height: 40px; vertical-align: middle; font-size: 2em;">A-1</td> <td></td> <td></td> </tr> </table>	NTIS	GRAM	<input checked="" type="checkbox"/>	DTIC	TRAC	<input checked="" type="checkbox"/>	UNANNOUNCED		<input type="checkbox"/>	JUSTIFICATION			DISTRIBUTION	AVAILABILITY AND/OR SPECIAL		A-1			<div style="border: 1px solid black; height: 150px; margin-bottom: 10px;"></div> <p style="text-align: center;">DATE ACCESSIONED</p> <div style="border: 1px solid black; height: 80px; margin-bottom: 10px;"></div> <p style="text-align: center;">DATE RETURNED</p> <div style="border: 1px solid black; height: 80px;"></div> <p style="text-align: center;">REGISTERED OR CERTIFIED NUMBER</p>	
NTIS	GRAM	<input checked="" type="checkbox"/>																		
DTIC	TRAC	<input checked="" type="checkbox"/>																		
UNANNOUNCED		<input type="checkbox"/>																		
JUSTIFICATION																				
DISTRIBUTION	AVAILABILITY AND/OR SPECIAL																			
A-1																				
<p>DISTRIBUTION STAMP</p> <p style="font-size: 2em; margin: 20px 0;">19970114 019</p>																				
<p>DATE RECEIVED IN DTIC</p> <p>PHOTOGRAPH THIS SHEET AND RETURN TO DTIC-FDAC</p>																				

HANDLE WITH CARE

DISCLAIMER NOTICE



THIS DOCUMENT IS BEST QUALITY AVAILABLE. THE COPY FURNISHED TO DTIC CONTAINED A SIGNIFICANT NUMBER OF COLOR PAGES WHICH DO NOT REPRODUCE LEGIBLY ON BLACK AND WHITE MICROFICHE.

UNCLASSIFIED

LATERAL JET EFFECTIVENESS STUDIES FOR A MISSILE USING NAVIER-STOKES SOLUTIONS

B. Srivastava*
Raytheon Co., Raytheon Electronic Systems
Tewksbury, MA

Abstract

Several 3-D, viscous, turbulent Navier-Stokes computations have been performed for a missile equipped with and without divert jet thruster for three different wing planforms (having a fixed tail configuration) at a nominal flow Mach number of 3.94, angles-of-attack ranging from 2 to 25 deg and jet thrust ratios of one and four. Results are presented to show that the normal force and pitching moment coefficients for all computed cases are predicted within 5 percent of the wind-tunnel data. Synthesis of all the results show low amplification factor for all windward jet thruster cases. For this case the upstream favorable pressure zone created by the windward jet is insufficient to compensate for the massive unfavorable pressure loss on the windward wings/tails due to the jet blockage and jet wrap-around effects.

Nomenclature

AF Amplification Factor,
 $1 + (CN_{jet} - CN_{no-jet})/(T/q \cdot S)$
Alpha Angle-of-Attack (deg)

*Senior Development Engineer
System Design Laboratory,
Senior Member, AIAA

CN Normal Force Coefficient,
 $CN = (N/q \cdot S)$
dp Pressure Differential,
 $dp = (P_{jet} - P_{no-jet})/\Gamma \cdot P_{inf}$
Gamma Ratio of Specific Heats
M Freestream Mach Number
N Normal Force (N, lb)
P Pressure (N/m^2 , lb/ft^2)
Phi Azimuth Angle (deg)
q Dynamic Pressure, $q = 1/2 \rho v^2$
S Missile Cross-Sectional Area
(m^2 , ft^2)
T Jet Thrust (N, lb)
v Velocity (m/sec, ft/sec)

Greek

α Angle-of-Attack (deg)
 ρ Density
 ϕ Azimuth Angle (deg)

Subscript

inf Freestream condition
jet Condition with jet
no-jet Condition with no jet

Introduction

Rapid airframe response time is critical during the homing phase of interceptor missiles. Surface mounted, fast-reacting jet thrusters offer an attractive alternative to conventional aerodynamic surface control for improved missile agility and maneuverability. Performance enhancements at low speed and high altitude (where dynamic pressure is low) are additional advantages of the surface reaction jets. It has been found that under some missile orientations and flow conditions, the surface mounted lateral jet leads to

thrust amplification due to a high surface pressure region that forms ahead of the jet on the missile surface. Effective exploitation of the thrust amplification can lead to improved missile performance. However, it has also been observed that at certain other flow conditions and orientations, the reaction jets can produce negative effects (i.e., thrust deamplification). An understanding of the controlling factors that produce high amplification as well as those that produce low amplification are critical in developing a credible design basis for optimal missile performance.

The problem of the lateral jet interaction with the external flow, under conditions of varying flight Mach numbers, angles-of-attack and jet orientations, is extremely complex in nature and has been studied experimentally and analytically for many years^{1,2}. More recently, Computational Fluid Dynamics (CFD) studies³⁻⁷ have been performed to understand these effects. Our approach is to judiciously combine wind-tunnel testing and CFD simulation in an effort to evolve a validated design and analysis tool that can synthesize the physical complexity of the flow and identify its key controlling parameters. This paper deals with the overall CFD validations with and without lateral jet thrusters and subsequently outlines the utility of the approach for lateral jet effectiveness studies in relation to a missile design.

This paper is subdivided into several sections. The next section briefly outlines the previous work in this area using CFD approaches. The details of the computational methodology, geometry, grid related issues and boundary conditions for the CFD application are discussed later. CFD validation studies for a generic class of missile airframes with and without lateral thrusters

are then compared with the wind-tunnel data for the normal forces and moments. A later section presents the overall summary and conclusions for the paper.

Background

The topic of jet interaction with an external supersonic flow dates back to the mid-1960^{1,2}, when a large number of generic experimental data were generated and related correlation techniques were developed. Emergence of hypersonic interceptors, maturity of CFD and the advent of supercomputers revived these activities in the late 1980's³⁻⁷. Several investigators have performed CFD studies for the fundamental problem of jet interaction in relation to adaptive gridding⁸, turbulence models⁹, grid refinements¹⁰, and the impact of artificial viscosity⁸. These studies range from Euler¹¹ to Navier-Stokes computations¹². Of these studies, particular reference is made to the studies reported by Dash et.al.¹² and York et.al.⁶ because much of the current CFD effort is derived from their mature technical expertise in this area. Further details of the methodology and related research work can be obtained from the references cited.

While a vast number of numerical studies have been performed using controlled jet interaction studies for methodology development, efforts to simulate missile surfaces have been rather limited. More recently, Chan et.al.¹³ performed a series of studies that lead to the simulation of a full missile surface with control surfaces and jet interaction. Qin and Foster¹⁴ also performed similar studies using a Navier-Stokes approach for an inclined jet on an ogive/cylinder body. These results depict the remarkable flow details obtained using CFD approaches,

which ultimately result in making judicious choices for flight vehicles design and further wind-tunnel testing. Srivastava¹⁵ performed full Navier-Stokes studies for generic missile bodies with/without leeward and windward jets but without wing or tail panels. Comparisons with the wind-tunnel data, however, was not direct because the tests were conducted with tail panels while computations were performed without tail. Removal of the tail load from the wind-tunnel data by an approximate method introduced uncertainties that were not fully quantified. This deficiency in the CFD model has been eliminated in the current paper, which shows direct comparison of the CFD predictions with the wind-tunnel data by modeling all geometrical aspects of the wind-tunnel missile geometry.

Computational Methodology

PARCH⁶, which is a full Navier-Stokes (FNS) code with plume/missile airframe steady-flow predictive capability, is being used for our current studies. PARCH code utilizes formulations based on the NASA/Ames ARC aerodynamic code and the AEDC propulsive extension, PARC. This code is particularly suited for missile surfaces due to its grid patching capability which is useful for treating embedded surfaces in a flow field. Patching, that is accomplished in mapped computational coordinates, is automatically constructed from boundary inputs. Boundary conditions are applied along the outer computational boundaries and relevant embedded surfaces. The code utilizes diagonalized Beam-Warming numerics with matrix-split finite rate chemistry. Several versions of the K-E turbulence model are available in the code that were specifically developed for jet interaction and

propulsive studies. We are currently using the capped low Reynolds number formulation of Chien's K-E model¹² for the current simulations. Further details of the code capability can be found in Reference 6.

Typical boundary approaches for the current application (supersonic flows) are specified supersonic freestream conditions at the inlet and outer boundaries. Extrapolation procedures are employed at the exit boundary. Surface conditions are appropriate to viscous flows with adiabatic wall condition.

Surface jet boundary condition is the specified jet nozzle supersonic exit conditions. The circular area of the jet in the wind-tunnel test is approximated by a square aperture in the CFD simulation.

Fig. 1 shows a sketch of the wind-tunnel models recently tested by Raytheon in McAir Polysonic Wind-Tunnel with three different wing planforms. The wing in Fig. 1a is the baseline configuration which is 15.734 in. long and its leading edge starts at 12.134 in. from the missile nose. The jet thruster is located at 14 in. from the nose. The jet area is 0.1764 in.² circular hole. The second configuration, shown in Fig. 1b, is a forward wing configuration whose length remains the same but its leading edge is moved forward to 10.301 in., from the missile nose. The third configuration is a short wing, length 7.67 in. with leading edge starting at 10.301 in.. For all these configurations, tail panel geometry as well as the axial jet location are the same. Missile is rolled in the tunnel to achieve windward and leeward jet orientations. The full CFD simulation geometry is shown in Figs. 2-4 for the three configurations. CFD simulations utilize the rotation of inlet velocity vector to simulate leeward and windward jet orientations. These simulations were performed on three different grids corresponding to each configuration. The

UNCLASSIFIED

axial distribution of the grid was the only component that was modified keeping the total number of grids the same, i.e., 231*51*69, axial, normal and circumferential in that order. Grid patching procedure was used to apply the relevant boundary conditions on the surfaces. All angles-of-attack for a given configuration were simulated on a single grid consistent with the minimum desired Mach number and maximum desired angle-of-attack. This allows us to minimize on the grid effort. The grids were generated through 'GRIDGEN', with geometry models developed within 'GRIDGEN'¹⁶.

The jet area was resolved by using a 10 x 10 grid on the missile surface. The boundary conditions on this jet area grid were specified by inputting the exit conditions of a nozzle analysis using an iterative procedure consisting of the nozzle exit area, isentropic conditions and the specified jet thrust. Local time stepping procedures with conventional dissipation factors were employed to achieve convergence defined by at least three orders of magnitude reduction in the maximum residual. Converged solutions were checked with three and four orders of magnitude reduction in the maximum residual for selected cases. The minimum grid spacing near the missile surface was assigned by choosing a y^+ value of 5 for all computations. Variation of this value did not produce any significant changes in the predicted results. Post-analysis of the computed cases later suggested that the external flow is primarily supersonic and the vortical flow nature around the missile geometry is primarily governed by the inviscid phenomena. Selected test cases with inviscid CFD simulations showed that force and moment coefficients can be well predicted using inviscid models.

Comparison With Wind-Tunnel Tests

Our current effort was confined to a nominal flow Mach number of 3.94 with angles-of-attack varying from 2 to 25 deg. Exact wind-tunnel conditions were used for each CFD simulation. CFD efforts were restricted to leeward and windward jet orientations, which encompass the most severe flow cases. This also allows us to exploit symmetry in CFD simulation. Jet thrusts were simulated at the wind-tunnel test conditions of 175 and 50 lb (nominal cases).

Baseline Wings

Windward Jets

Fig. 5a shows the computed surface pressure contours for two cases. The top figure is with a windward jet, jet thrust 175 lb, at a flow Mach number of 3.94 and at an angle-of-attack of 20 deg. For this case, notice the extent of high pressure forward of the jet and very low pressures aft of the jet on the windward side. It is quite clear from this figure that the presence of the jet-on the surface has totally wiped out the aft normal forces created by the windward wings. This is more clear if we compare the lower figure which shows jet-off pressure contours, with the jet-on upper figure. The table on this figure shows the comparison of the normal force and pitching moment coefficients with the wind-tunnel data. The comparisons are excellent. Overall we can conclude from this figure that:

- (1) Windward located jet thruster creates a favorable high pressure zone

- ahead of the jet, but only at the expense of a massive loss of normal force from the windward wings.
- (2) For this case the thrust amplification factor (defined as $1 + \text{aero-interactive force/thrust}$, $\text{aero-interactive force} = \text{jet-on normal force on the airframe} - \text{jet-off normal force on the airframe}$) is 0.56. Note, however, that the pitching moment is significantly increased with the jet thrusters. Even though the latter can be used effectively to our advantage for vehicle maneuver, our goal is to also enhance the amplification factor.
 - (3) Notice also from these figures that a jet wrap-around effect is seen to create an adverse effect causing undesirable normal forces.
 - (4) The effect of the jet gas on the tail panels is also massive, resulting in the loss of tail control power for this jet orientation

These effects were observed in our previous computations⁴ but now the results are far more credible due to the excellent comparisons with the wind-tunnel data.

The vortical flow pattern of the missile with and without the windward jet can be observed from Figs. 5b-5f. In Fig. 5b, the total pressure contours for several axial locations of the missile without the divert thruster is shown. Notice the early formation of the body vortices on the leeward side, forward of the wings, which interact with the leeward wings, are subsequently modified and later interact with the tail panels. Additional vortices are generated on the leeward side of the lower wings that later follow an upward path as seen from this figure. Fig. 5c shows the Mach number

contours for the same axial locations as in Fig. 5b showing fully supersonic flows for the entire flow field. For these flow conditions, the inviscid effects dictate the vortical flow structure.

Figs. 5d-5f show similar plots with a windward divert thruster. Notice from these figure that the jet effects result in massive loss of the total pressure, first on the windward side but gradually wrapping around the missile downstream to engulf the leeward side of the missile surfaces.

Fig. 6 shows similar computations for a lower jet thrust of 50 lb at identical flow conditions. Once again, first observe the excellent comparison with the wind-tunnel data. For this case the thrust amplification factor is -0.17, indicating that the thruster loses its effectiveness except for the gains in the moment coefficient. Figs. 7a and 7b show the previous results in a different format. In an effort to enhance the interactive effects, a pressure differential plot between the jet-on and jet-off cases are shown for high and low thrust cases. Note from these figures that the high pressure zone ahead of the jet, wrap-around effects of the jet and massive loss of pressure forces on windward wing and tail panels are the controlling physical mechanisms.

At a jet thrust of 175 lb, the effect of angles-of-attack are shown in Figs. 8 and 9. Note that at an angle-of-attack of 10.8 deg, comparisons with wind-tunnel remain excellent and the forward high pressure interactive zone seems to shrink in extent especially in the front end. This is more visible in Fig. 9 for angle-of-attack of 4.02 deg with excellent comparisons with the wind-tunnel data.

Further computations were made for angles-of-attack of 9.95 and 3.13 deg without the jet thrusters to validate the CFD

UNCLASSIFIED

results at low angles-of-attack. These results are shown in Figs. 10 and 11. Predicted results are in excellent comparison with the experimental data.

Leeward Jets

Figs. 12-15 show the CFD computations for leeward jet orientation. Two thrust levels were computed, 175 and 50 lb. The angle-of-attack range was from 2.2 to 20 deg at a nominal flow Mach number of 3.94. All the computed results, as shown in these figures, show excellent comparisons with the wind-tunnel data. Fig. 12a shows two views of the computed results for a jet thrust of 175 lb at an angle-of-attack of 19 deg. View I shows the leeward side while view II shows the windward side. A comparison of this figure with the results shown in Fig. 5 show the following:

- (1) For a leeward jet thruster, there is only a marginal positive pressure gain ahead of the jet because the jet exhausts in a vortical flow zone.
- (2) The windward wings and missile body pressure levels are also affected, as is seen if we compare Fig. 12a view II, with the jet-off windward side in Fig. 5.
- (3) Comparison with the experimental data is excellent

Figs. 12b-12d show the vortical flow pattern for the leeward divert thruster. Notice from the total pressure contours of Fig. 12b that the effect of the leeward jet is confined between the two leeward wings. Comparison of this figure to Fig. 5b (without the divert thruster), shows that the windward flow pattern for the two cases are very similar. This indicates that for leeward jets,

jet effects are confined only to the leeward side of the missile surfaces. Fig. 12d shows the Mach number contours for this case showing predominantly supersonic flow everywhere in the flow field.

Fig. 13 shows a similar comparison for a leeward jet with a jet thrust of 50 lb and an angle-of-attack of 20 deg. The table shows the excellent comparison of the computed results with the experimental data. Notice also from this figure that the windward control surfaces are nearly unaffected by the presence of the leeward jets. Figs. 14 and 15 show that at lower angles-of-attack, 9 and 2.2 deg, respectively, the positive pressures ahead of the leeward jets are somewhat recovered due to the interaction with approaching streamlines over the missile body.

Forward Wings

In an attempt to understand the effects of the jet thruster location in relation to the missile wings, tests were conducted with wings moved forward of the jet location by 1.83 in. The objective was to attempt to enhance the positive pressure effects forward of the jets, for windward jet orientation, in an effort to enhance amplification factors. Fig. 16 shows the computations with a forward wing, with and without windward jets, at an angle-of-attack of 25 deg and a nominal flow Mach number of 3.94. Once again, the excellent comparisons between the computed results and wind-tunnel data is obvious from the table on this figure. It is also observed from this figure that with a forward wing, the positive pressure zone is somewhat larger as compared to Fig. 5 for the baseline wing (note that the angle-of-attack is lower in Fig. 5). The amplification factor for this case is 0.47. This happens because the loss of positive pressure on the

windward wings due to the jets effects still dominates the gain ahead of the jet. This phenomena persists at a lower jet thrust level of 102 lb for this case as shown in Fig. 17.

Short Wings

A short wing (length 7.672 in. as compared to baseline case of 15.734) missile was also tested in the wind-tunnel to investigate jet effects. Fig. 18 shows the computed results for this case at an angle-of-attack of 20 deg and a flow Mach number of 3.94, with and without jet effects. The overall CFD comparisons for normal and pitching moment coefficients are still excellent, as shown in the table on this figure. The amplification factor for this case is 1.12 which compares to 0.56 for the baseline wing at the same condition. It would appear, at least superficially, that significant gains in amplification factor may be achieved by careful selection of wing planform and the location of the lateral jet relative to the wing. The same behavior is observed in Fig. 19 at a reduced jet thrust level of 50 lb. In Fig. 20, the pressure differential between the jet-on and the jet-off conditions are shown for the short wing. This figure highlights the jet wrap-around effect and loss of tail load with the jet-on conditions.

Rolled Baseline Wings

When the missile is rolled such that one of the wings is vertically downward, the vortical flow pattern is likely to be influenced. The computational results and comparison with experiments for this missile orientation is discussed next.

Fig. 21a shows the computed pressure contours for this orientation of the missile at

an angle-of-attack of 20 deg and a flow Mach number of 3.94. This figure also shows the comparison of the experimental data with the computed force and moment coefficients. Notice that the experiments were at a slightly different condition that introduces asymmetry where as CFD computations were made for a symmetric case. A somewhat clear view of the pressure contours are shown in Fig. 21b. Notice that the horizontal wings are highly loaded for this orientation of the missile. Fig. 21c shows the total pressure contours indicating vortical flow pattern for this missile orientation while Fig. 21d shows the Mach number contours. Notice again the supersonic nature of the flow pattern for the whole flowfield.

Overall Results

All the predicted results from CFD and wind-tunnel tests for the normal force coefficients and the pitching moment coefficients are shown in Figs. 22 and 23, respectively, indicating the degree of deviation of the predicted results from the wind-tunnel data. Notice that both curves show very little deviation from the desired 45 deg line. The corresponding table of data is shown in Table. I.

Conclusions

Eighteen widely varying wind-tunnel test cases, encompassing geometry variations (baseline, forward and short wings), angles-of-attack (2 to 25 deg), lateral jet-on with windward and leeward orientations and jet-off, were simulated using CFD to show that the normal force and moment coefficients for all cases are in excellent agreement with the data. Fig. 22 for the normal force coefficient and Fig. 23 for the pitching moment coeffi-

UNCLASSIFIED

cient sum up the overall accuracy of the predicted results for all the cases considered. These validations demonstrate that our current CFD methodology can provide accurate predictions of the force and moment coefficients at widely varying flow conditions. Additionally, synthesis of the CFD results for various cases highlight the physical mechanisms that inhibit the jet amplification factor for windward jet orientation.

References

- 1) Cassel, L.A., Davis, J.G. and Engh, D.P., "Lateral Jet Control Effectiveness Prediction for Axisymmetric Missile Configurations," U.S. Army Missile Command, Redstone Arsenal, Alabama, Report #RD-TR-68-5, June, 1968.
- 2) Spring, Donald, "An Experimental Investigation of the Interference Effects due to a Lateral Jet Issuing from a Body of Revolution over the Mach No. Range of 0.8 to 4.5," U.S. Army Missile Command, Redstone Arsenal, Alabama, Report #RD-TR-68-10, Aug, 1968
- 3) Chamberlain, R., "Control Jet Interaction Flowfield Analysis," Lockheed Report LMSC F268936, Aerodynamic Investigations, Vol. 5, Feb, 1990
- 4) Chamberlain, R., "Calculation of Three-Dimensional Jet-Interaction Flowfields," AIAA Paper 90-2099, 1990
- 5) Weatherly, D., and McDonough, J., "Performance Comparisons of Navier-Stokes Codes for Simulating Three-Dimensional Hypersonic Crossflow/Jet Interaction," AIAA Paper 91-2096, 1991
- 6) York, B. J., Sinha, N., Kenzakowski, D.C. and Dash, S.M., "PARCH Code Simulation of Tactical Missile Plume/Airframe/Launch Interactions," 19th JANNAF Exhaust Plume Technology Meeting, May, 1991, CPIA PWB 568, pp. 645-674
- 7) Chan, S.C. and Roger, R.P., Edwards, G.L. and Brooks, W.B., "Integrated Jet Interactions CFD Predictions and Comparison to Force and Moment Measurements for a Thruster Attitude Controlled Supersonic Missile," AIAA Paper 93-3522, 1993
- 8) Lytle, J.K., Harloff, G.J. and Hsu, A.T., "Three-Dimensional Compressible Jet-in-Crossflow Calculations Using Improved Viscosity Models and Adapted Grid," AIAA Paper 90-2100, 1990
- 9) Dash, S.M., Sinha, N., York, B.J., Lee, R.A., and Hosangadi, A., "On the Inclusion of Advanced Turbulence Models and Nonequilibrium Thermochemistry into State-of-the-Art CFD Codes and Their Validation," AIAA Paper 92-2764, 1992
- 10) Rizzetta, D.P., "Numerical Simulation of Slot Injection into a Turbulent Supersonic Stream," AIAA Paper 92-0827, 1992
- 11) Darmieux, M. and Marasaa-Poey, R., "Numerical Assessment of Aerodynamic Interactions on Missiles with Transverse Jets Control," AGARD Meeting on Computational and Experimental Assessment of Jets in Cross Flow, April, 1993

UNCLASSIFIED

TABLE I - Table Showing Comparisons of CFD and Wind Tunnel Force
and Moment Coefficients

CASE #	Mach Number	Angle of Attack-deg	Jet Thrust T (Lb.)	CN CFD	CN EXPT.	CM CFD	CM EXPT.
1, BW	3.94	20	175	8.96	8.71	22.56	22.5
2, BW	3.94	20	0	7.3	6.8	5.96	5.97
3, BW	3.94	20	50	6.91	6.63	11.96	12.28
4, BW	3.94	10.8	175	6.54	6.30	16.03	15.76
5, BW	3.94	4.02	175	4.86	4.70	13.48	13.26
6, BW	3.94	9.95	0	2.83	2.84	2.71	2.89
7, BW	3.94	3.13	0	0.73	0.79	0.91	1.081
8, BW	3.94	19.0	-175	2.49	2.35	-6.09	- 6.20
9, BW	3.94	20.0	-50	5.55	5.46	2.15	2.24
10, BW	3.94	9	-175	-1.47	-1.4	-9.4	-9.09
11, BW	3.94	2.2	-175	-3.39	-3.3	-11.59	-11.37
12, FW	3.94	25.0	175	11.13	10.77	29.24	29.70
13, FW	3.94	25.0	0	9.28	9.17	11.03	11.66
14, FW	3.94	25.0	102	9.66	9.40	23.03	23.52
15, SW	3.94	20.0	175	9.31	8.97	25.11	25.32
16, SW	3.94	20.0	50	6.45	6.02	13.78	13.68
17, SW	3.94	20.0	0	5.53	5.15	7.65	7.49

NOTE:

BW - Baseline Wing
 FW - Forward Wing
 SW - Short Wing

 CN - $F_N / (q \cdot S)$
 CM - $F_N \cdot (X_{mc} - X_{cp}) / (q \cdot S \cdot X_{ref})$
 F_N - Normal Force (Lbs)
 q - Dynamic head
 S - Cylinder Cross- Sectional Area
 X_{ref} - Reference Length (Cylinder Diameter)
 X_{mc} - Moment Reference distance

UNCLASSIFIED

- 12) Dash, S.M., York, B.J., Sinha, N., Lee, R.A., Hosangadi, A., and Kenzakowski, D.C., "Recent Developments in the Simulation of Steady and Transient Transverse Jet Interactions for Missile, Rotorcraft, and Propulsive Applications," AGARD Meeting on Computational and Experimental Assessment of Jets in Cross Flow, April, 1993
- 13) Chan, S.C. and Roger, R.P., Brooks, W.B., Edwards, G.L. and Boukather, S.B., "CFD Predictions and Comparisons to Wind Tunnel Data for the Asymmetric Firing of a Forward Mounted Attitude Control Thruster," AIAA Paper #95-1895, June, 1995
- 14) Qin, N. and Foster, G.W., "Study of Flow Interactions due to a Supersonic Lateral Jet Using High Resolution Navier-Stokes Solutions," AIAA 94-2151, June, 1995
- 15) Srivastara, B., "CFD Analysis and Validation for Lateral Jet Control of a Missile," AIAA 96-0288, Jan, 1996
- 16) Steinbrenner, J.P. and Chawner, J.R., "Recent Enhancements to the GRID-GEN Structural Grid Generation System," Proceedings of the NASA Workshop on Software Systems for Surface Modeling and Grid Generation, Hampton, Virginia, April, 1992
- 17) Soni, B.K., Thompson, J.F. Stokes, M.L., and Shih, M.H., "GENIE⁺⁺, EAGLEVIEW and TIGER: General Purpose and Special Purpose Graphically Interactive Grid System," AIAA-92-0071, Jan, 1992

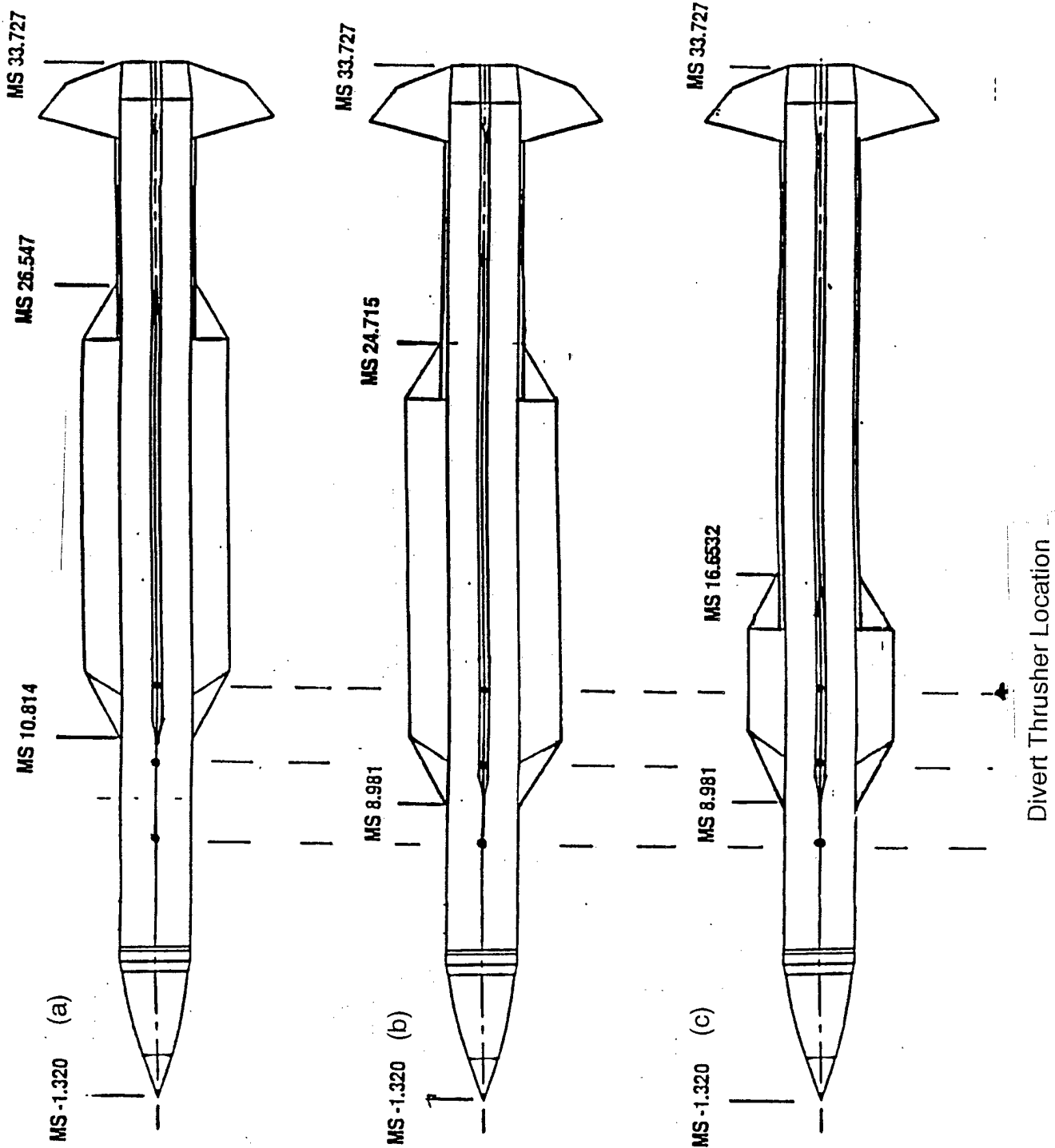
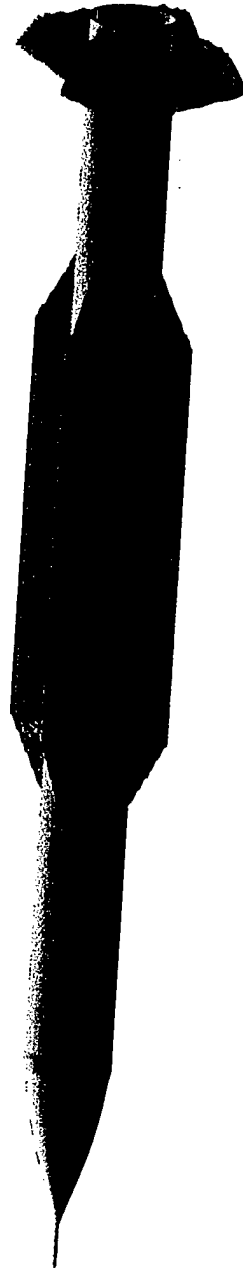
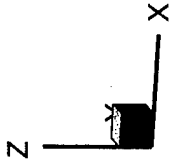


Fig. 1 - Missile Wind Tunnel Test Geometry

UNCLASSIFIED



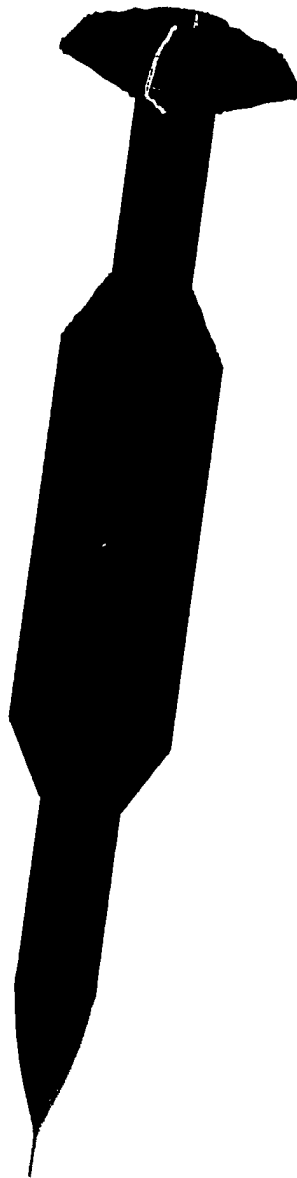
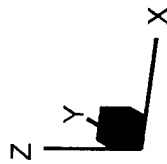
Baseline Wing Configuration

Wing Length - 15.734 inch

Leading Edge - 12.134 inch

Fig. 2 - Wind Tunnel Geometry for Computational Fluid Dynamics Simulation

UNCLASSIFIED



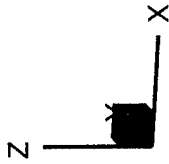
Forward Wing Configuration

Wing Length - 15.734 Inch

Leading Edge - 10.301 Inch

Fig. 3 - Wind Tunnel Geometry for Computational Fluid Dynamics Simulation

UNCLASSIFIED



Short Wing Configuration
Wing Length - 7.67 inch
Wing Leading Edge - 10.301 inch

Fig. 4 - Wind Tunnel Geometry for Computational Fluid Dynamics Simulation

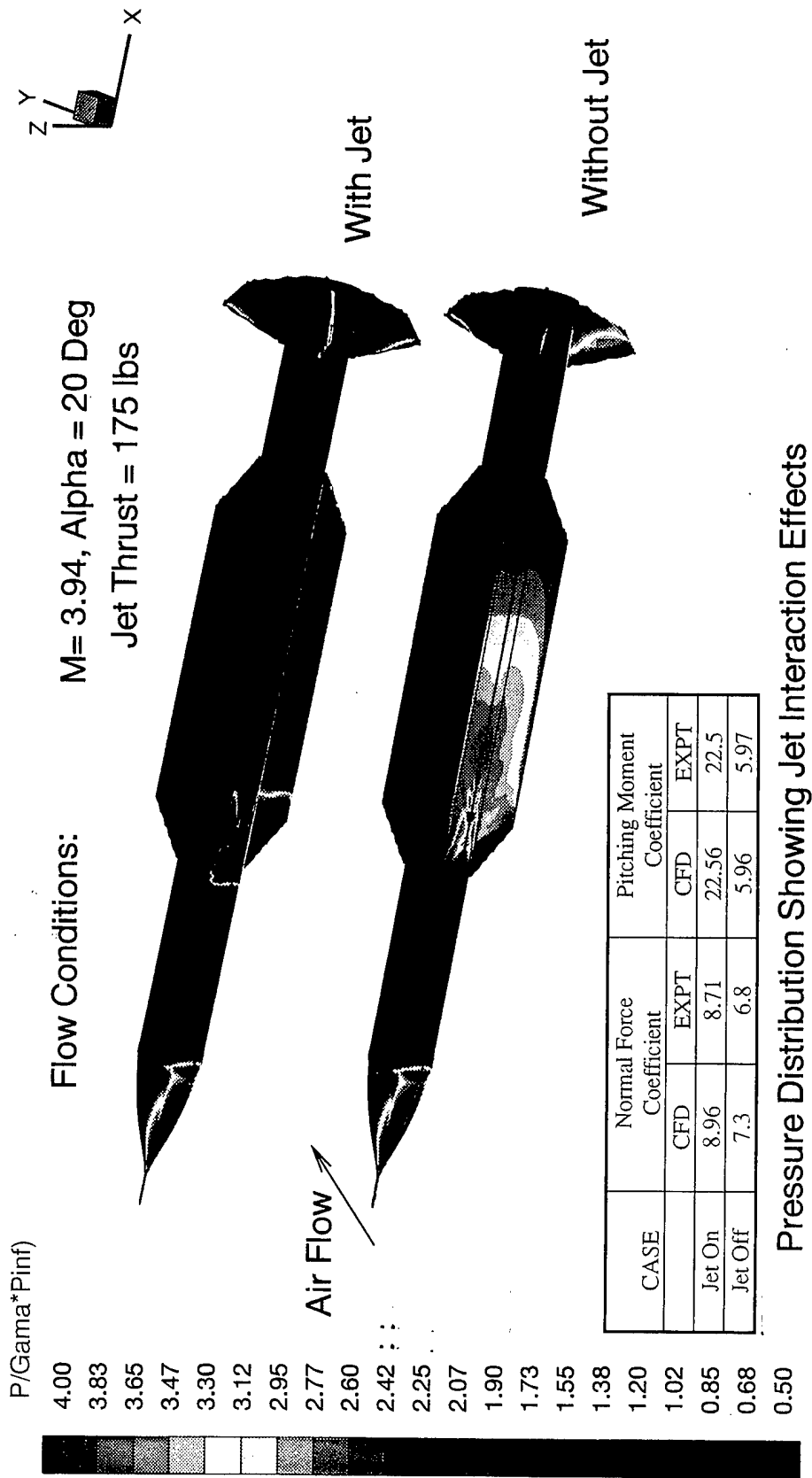
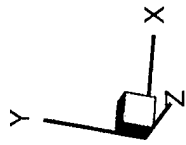


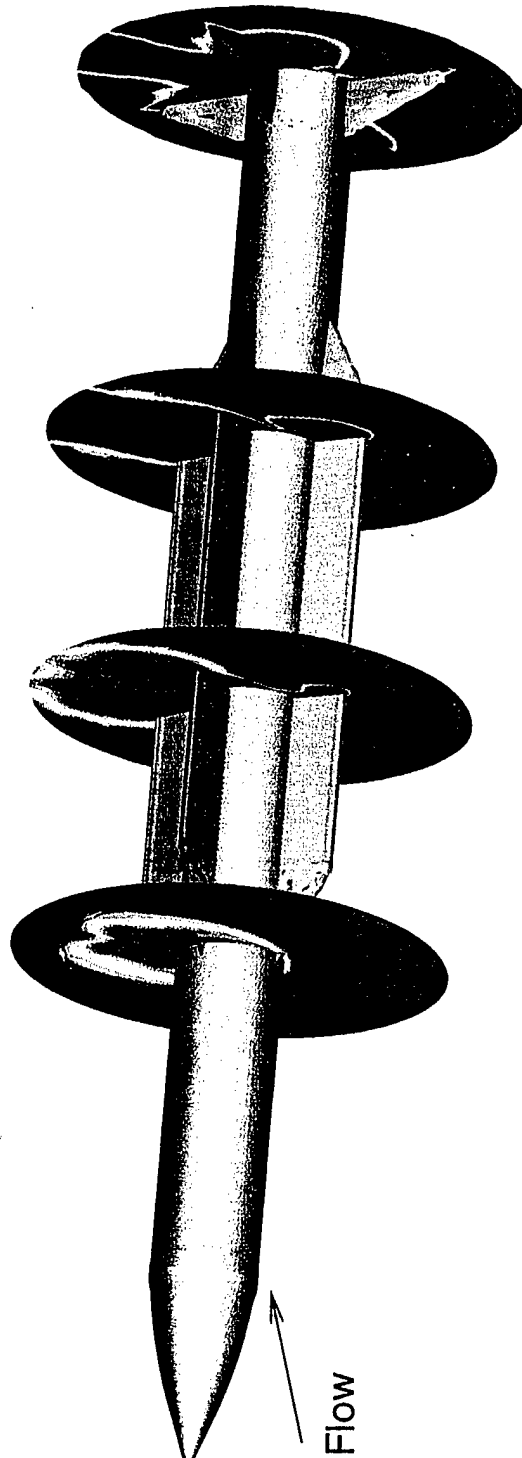
Fig. 5a - CFD Simulation of Wind Tunnel Geometry With Windward Jet



$P_0 / (\gamma \cdot p_{inf})$

70.00
66.75
63.50
60.25
57.00
53.75
50.50
47.25
44.00
40.75
37.50
34.25
31.00
27.75
24.50
21.25
18.00
14.75
11.50
8.25
5.00

Missile Without Thruster Jet



Flow Mach Number - 3.94

Angle of Attack- 20 Deg

Total Pressure Contours at Several Axial Locations Showing Jet Effects

Fig. 5b - CFD Simulation of a Missile With Wings, Tail Panels and Lateral Thruster Jet

UNCLASSIFIED

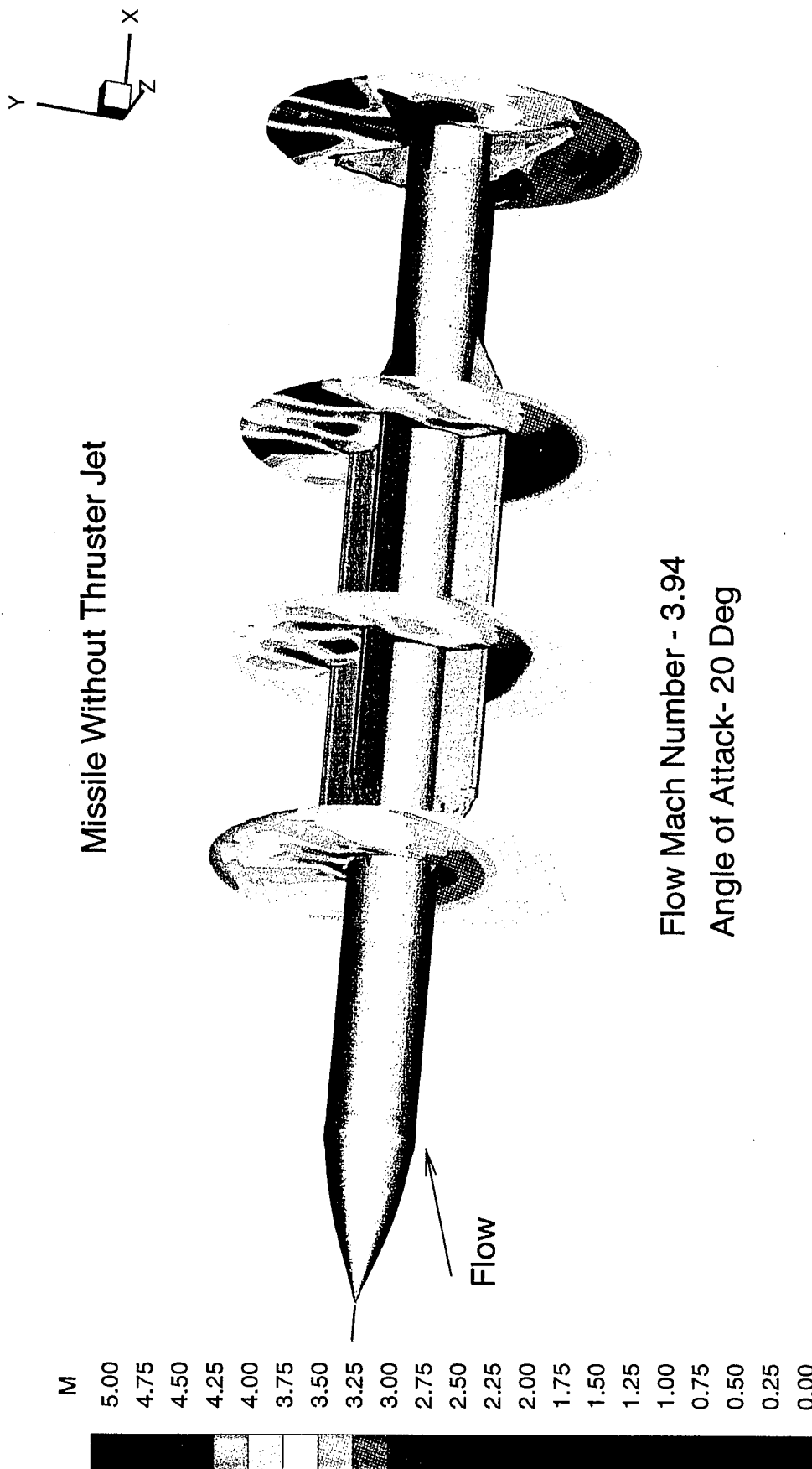


Fig. 5c - CFD Simulation of a Missile With Wings, Tail Panels and Lateral Thruster Jet

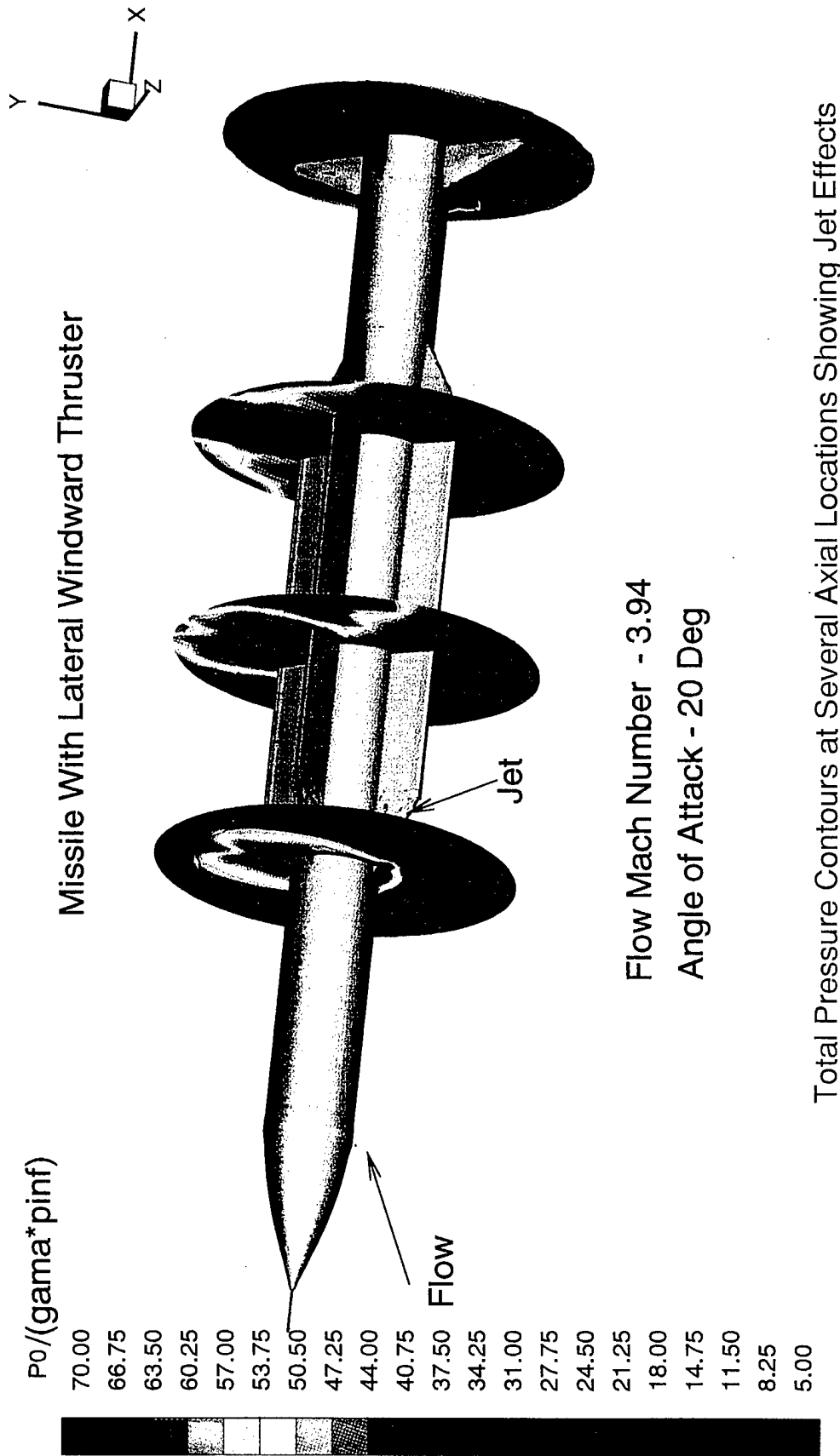
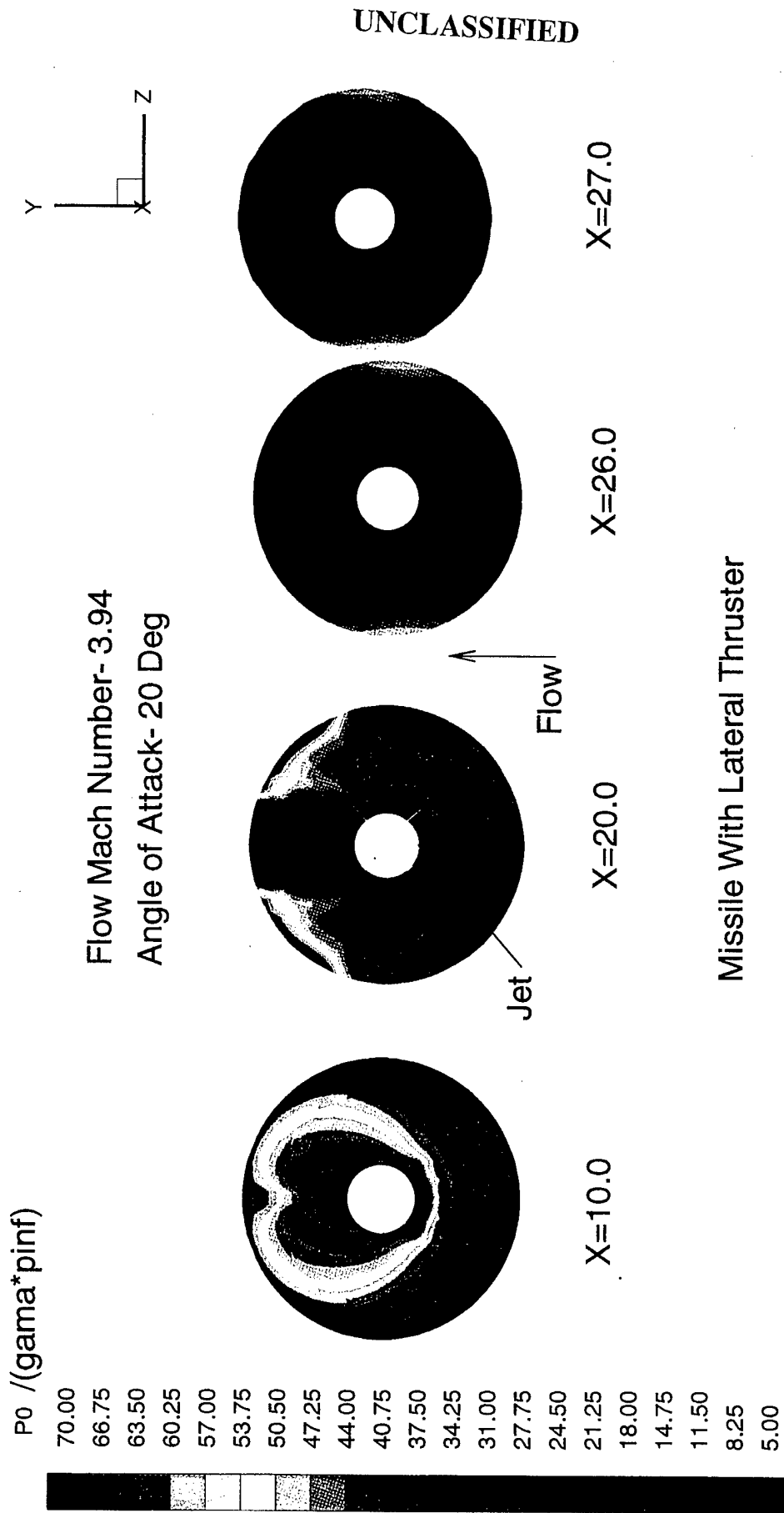
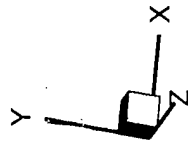


Fig. 5d - CFD Simulation of a Missile With Wings, Tail Panels and Lateral Thruster Jet

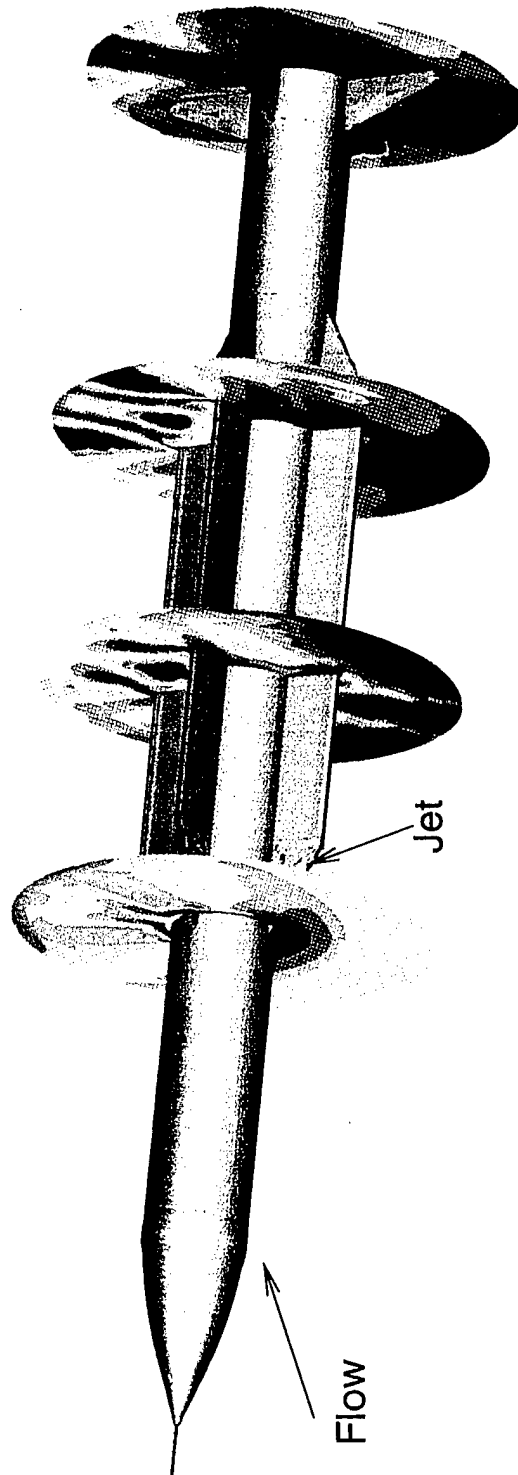
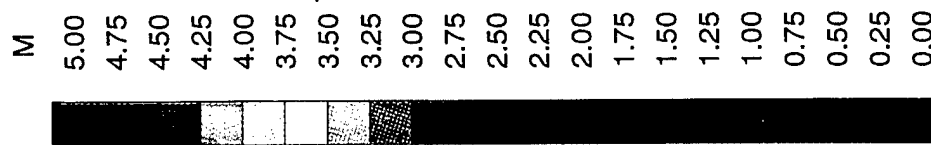


Total Pressure Contours at Various Axial Locations Showing Vortex Formation

Fig. 5e - Vortex Formation on a Missile With Wings, Tail Panels and Lateral Thruster Jet



Missile With Lateral Windward Thruster



Flow Mach Number - 3.94

Angle of Attack - 20 Deg

Mach Number Contours at Several Axial Locations Showing Jet effects

Fig. 5f - CFD Simulation of a Missile With Wings, Tail Panels and Lateral Thruster Jet

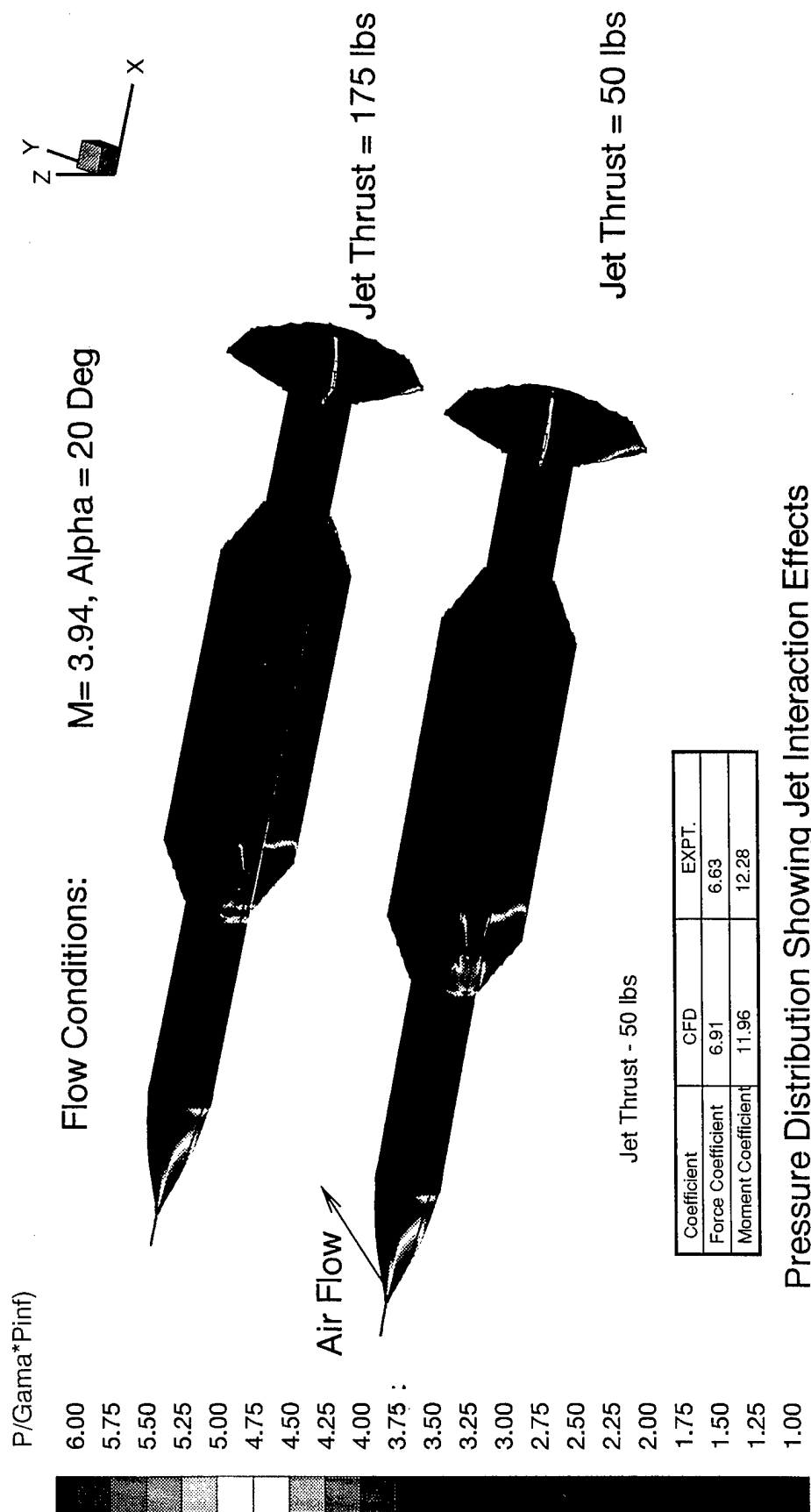


Fig. 6 - CFD Simulation of Wind Tunnel Geometry With Windward Jet

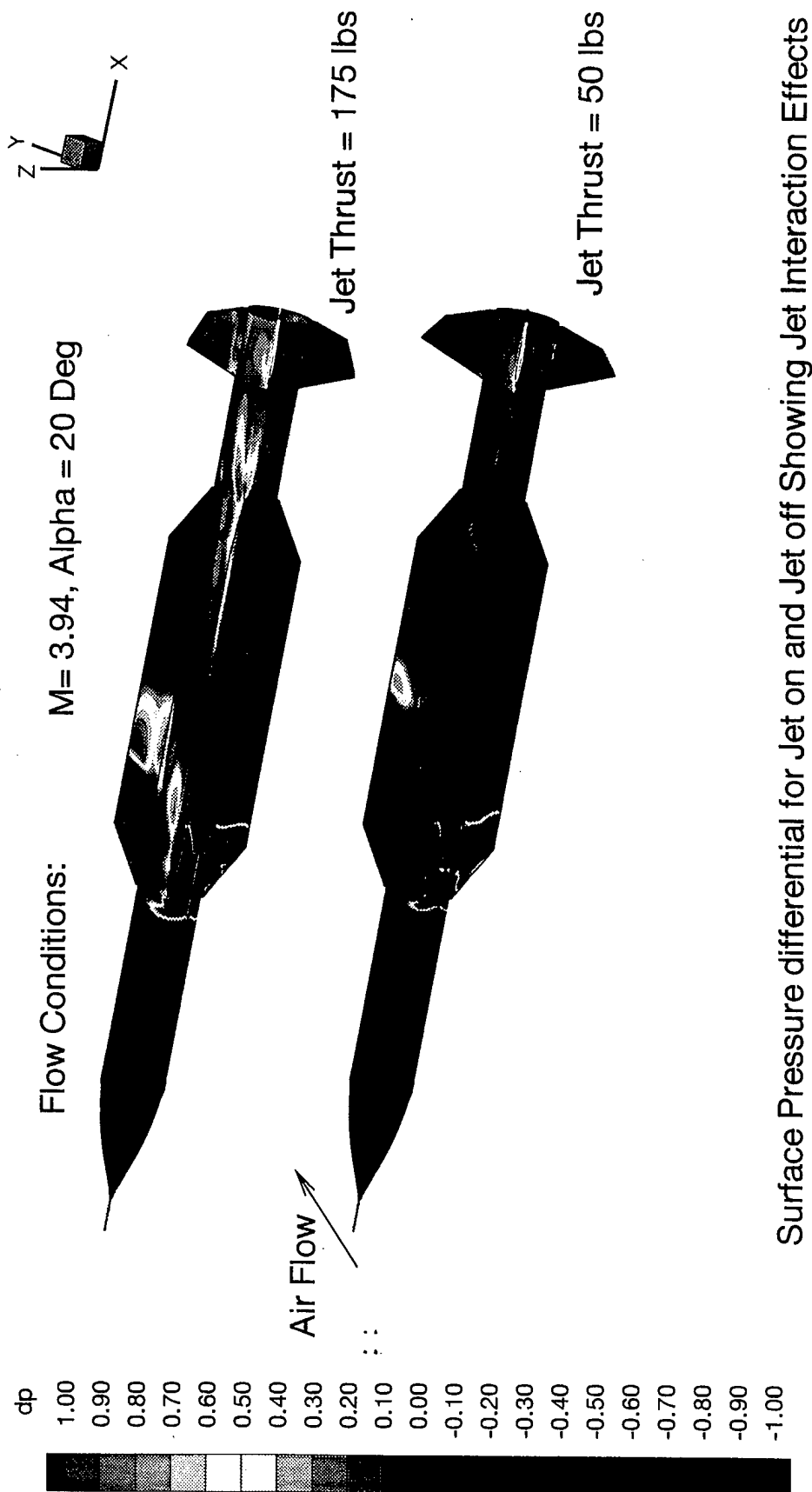


Fig. 7a - CFD Simulation of Wind Tunnel Geometry With Windward Jet

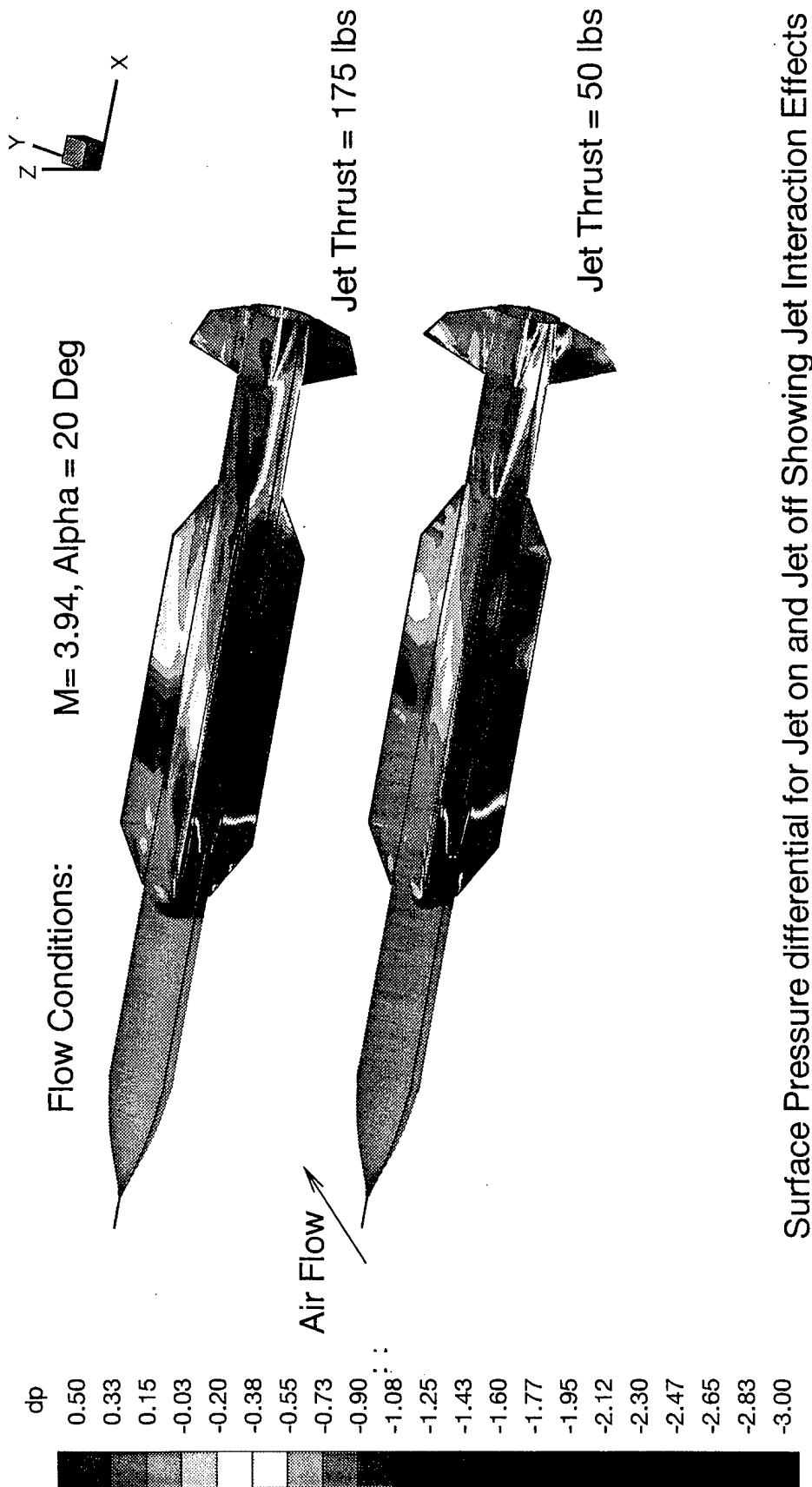
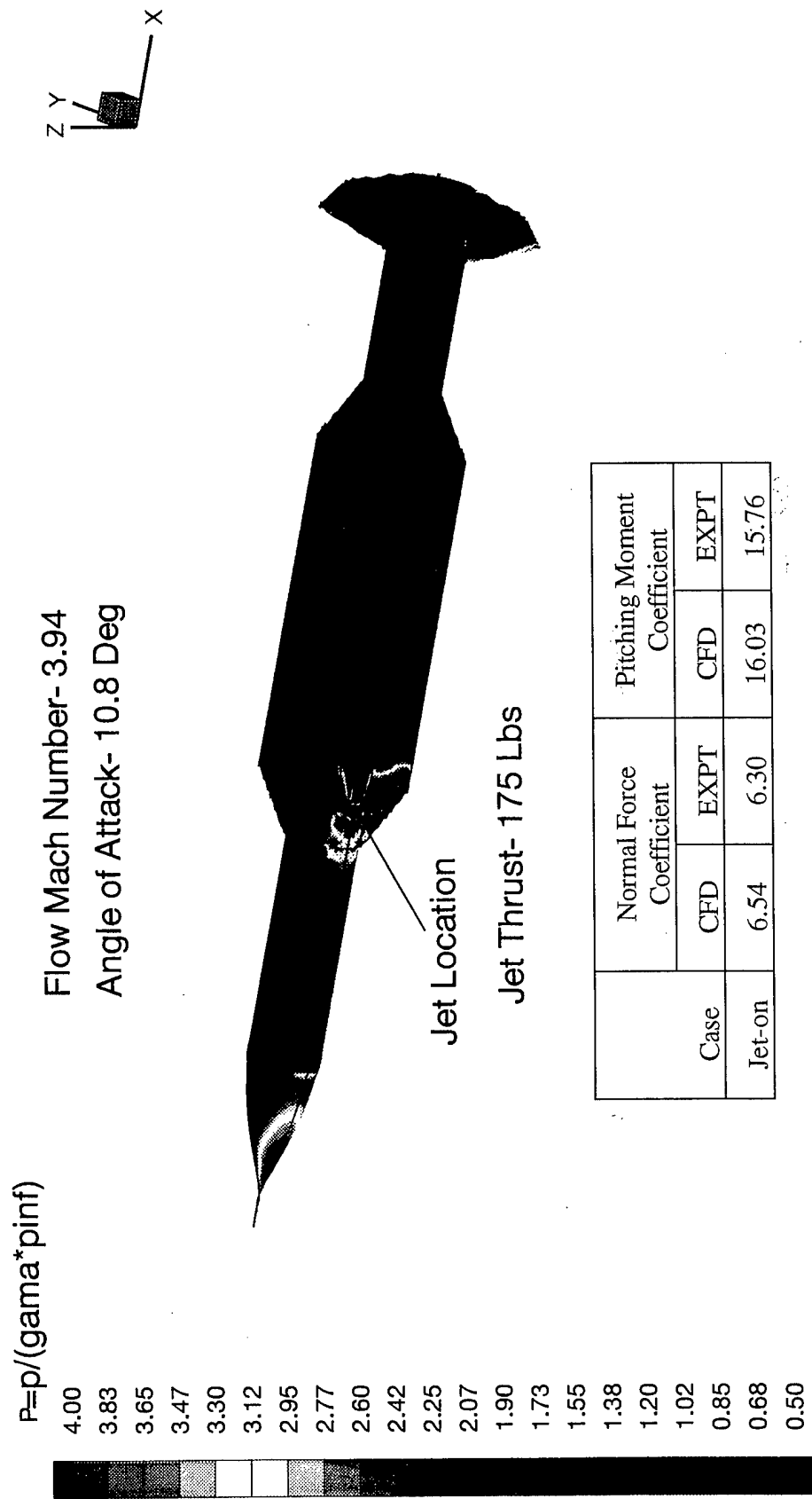
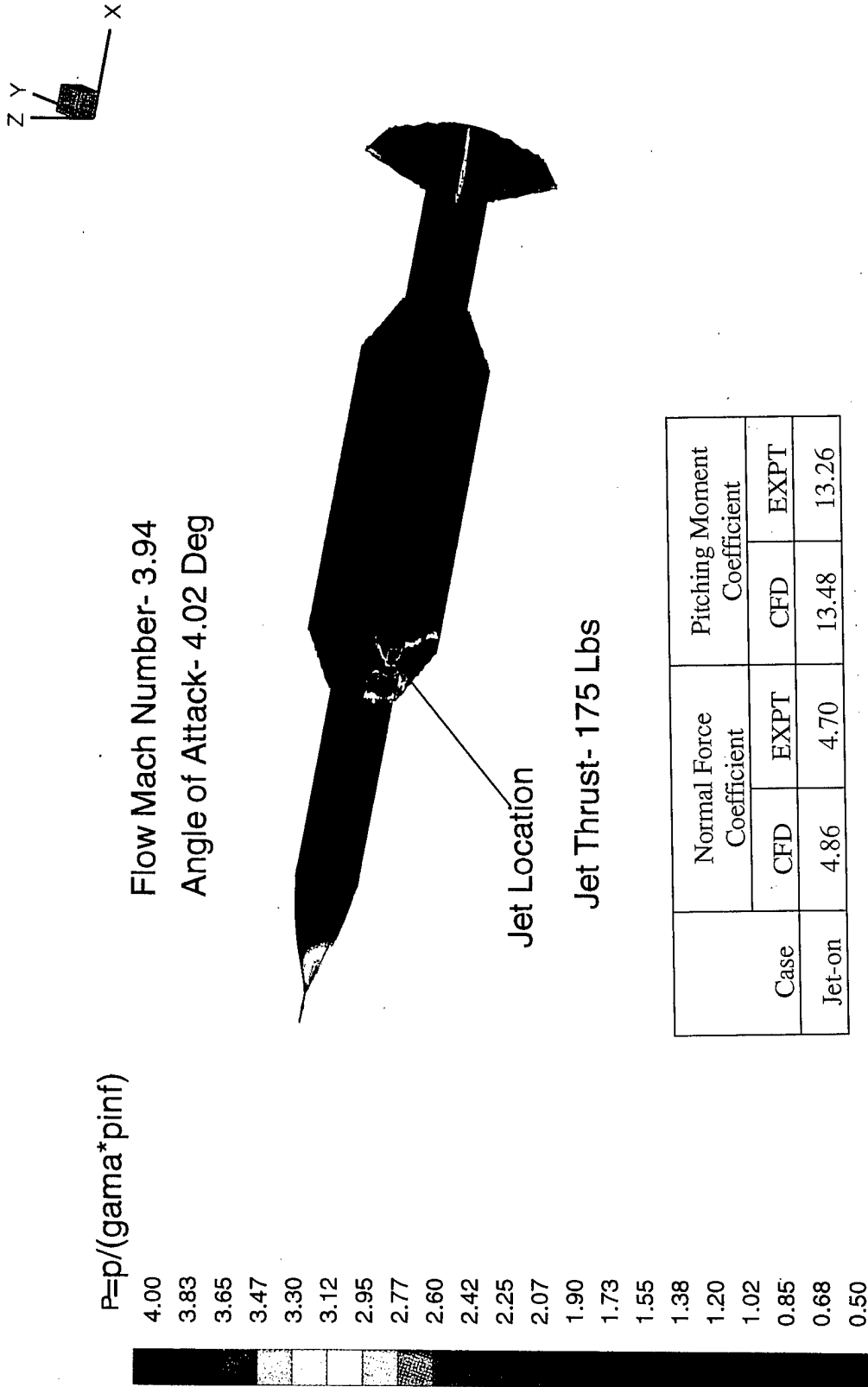


Fig. 7b - CFD Simulation of Wind Tunnel Geometry With Windward Jet



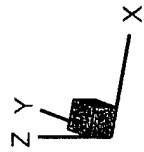
Missile Surface Pressure Distribution Showing Jet Interaction Effects

Fig. 8 - CFD Simulation of Wind Tunnel Geometry With Windward Jet



Missile Surface Pressure Distribution Showing Jet Interaction Effects

Fig. 9 - CFD Simulation of Wind Tunnel Geometry With Windward Jet



$P = p / (\gamma \rho a^2)$

4.00
3.83
3.65
3.47
3.30
3.12
2.95
2.77
2.60
2.42
2.25
2.07
1.90
1.73
1.55
1.38
1.20
1.02
0.85
0.68
0.50

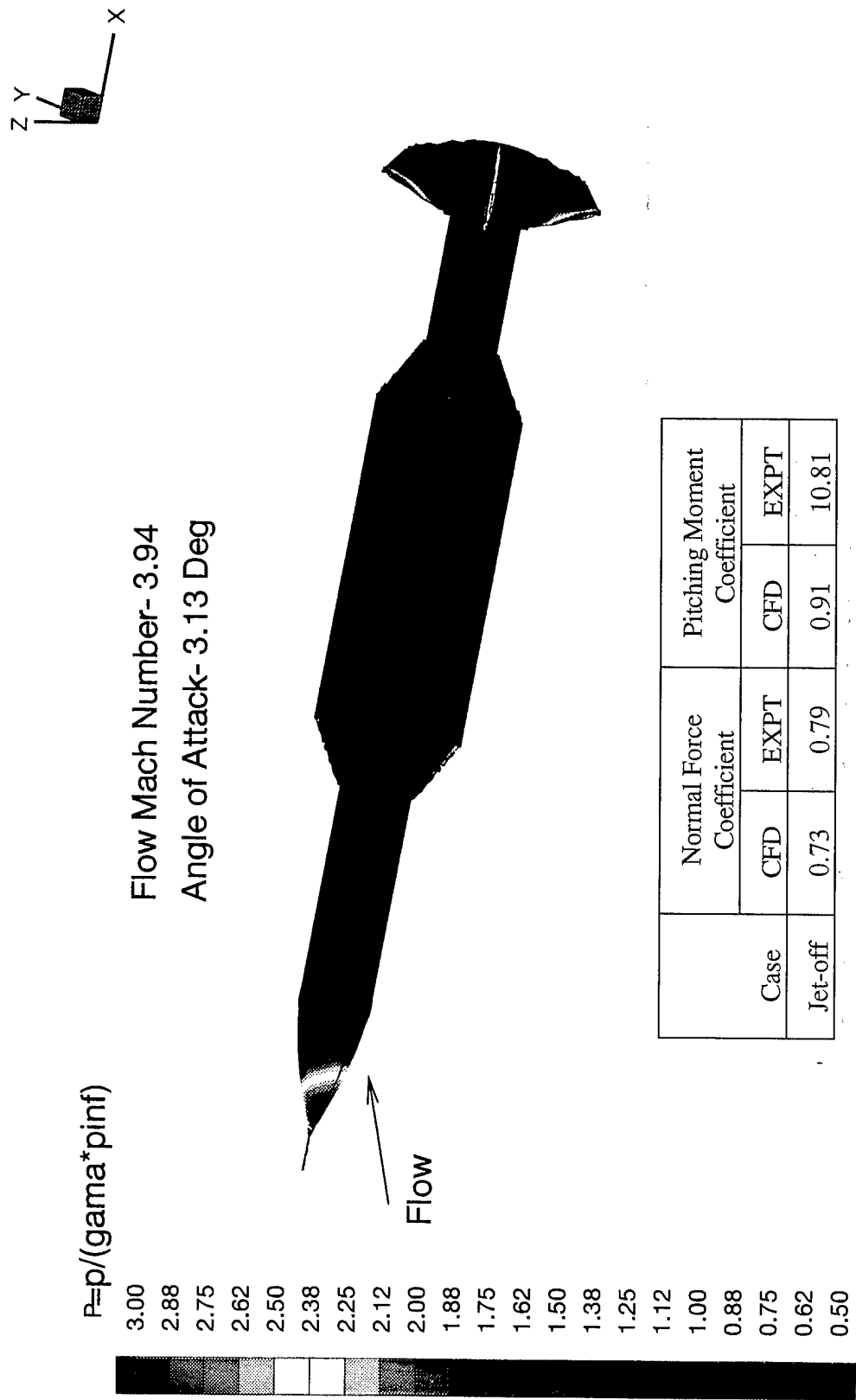
Flow Mach Number- 3.94
Angle of Attack- 9.95 Deg



Case	Normal Force Coefficient		Pitching Moment Coefficient	
	CFD	EXPT	CFD	EXPT
Jet-off	2.83	2.84	2.71	2.89

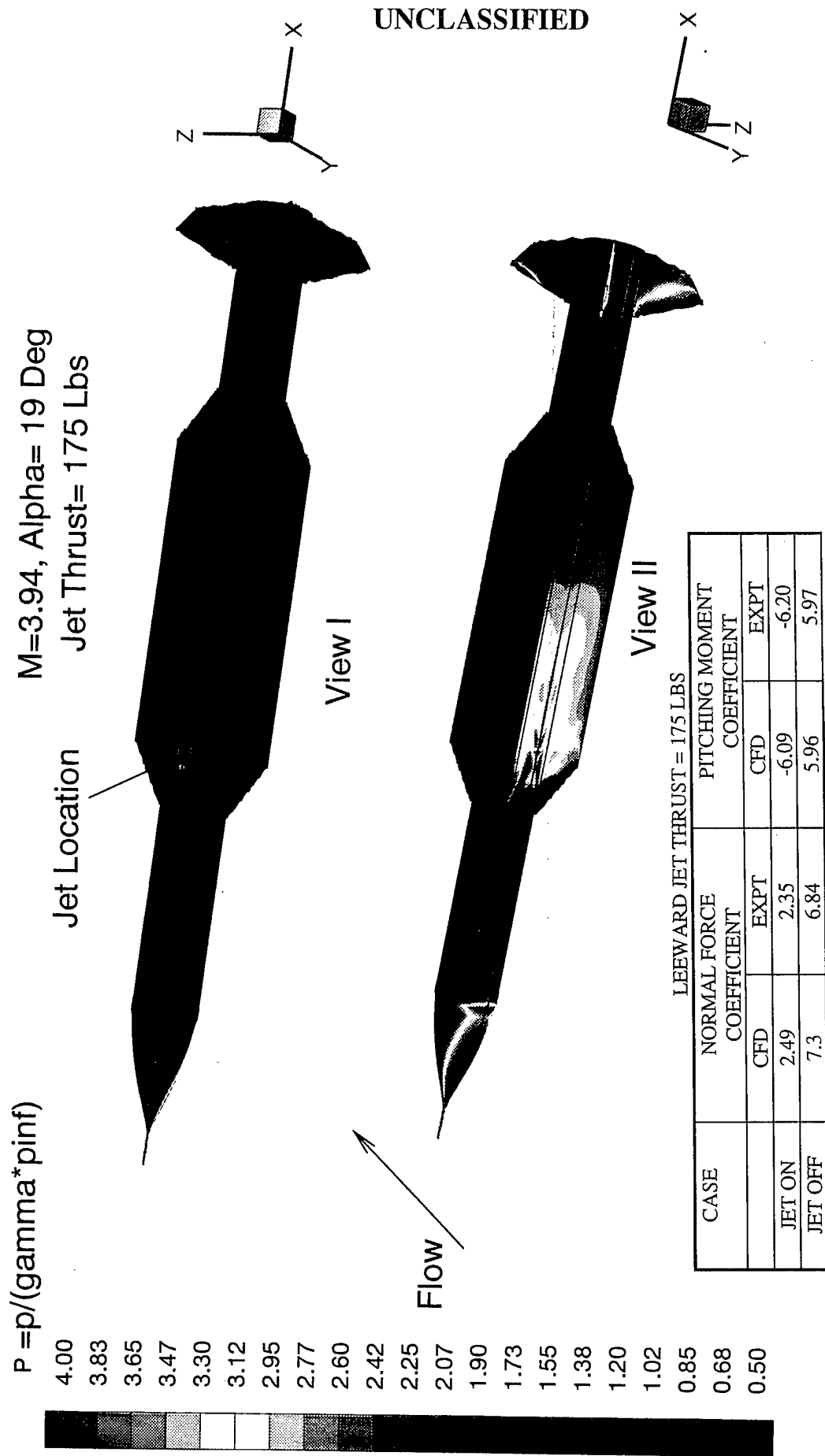
Missile Surface Pressure Distribution Showing Wings and Tail Loads

Fig. 10 - CFD Simulation of Wind Tunnel Geometry Without Jet



Missile Surface Pressure Distribution Showing Wings and Tail Loads

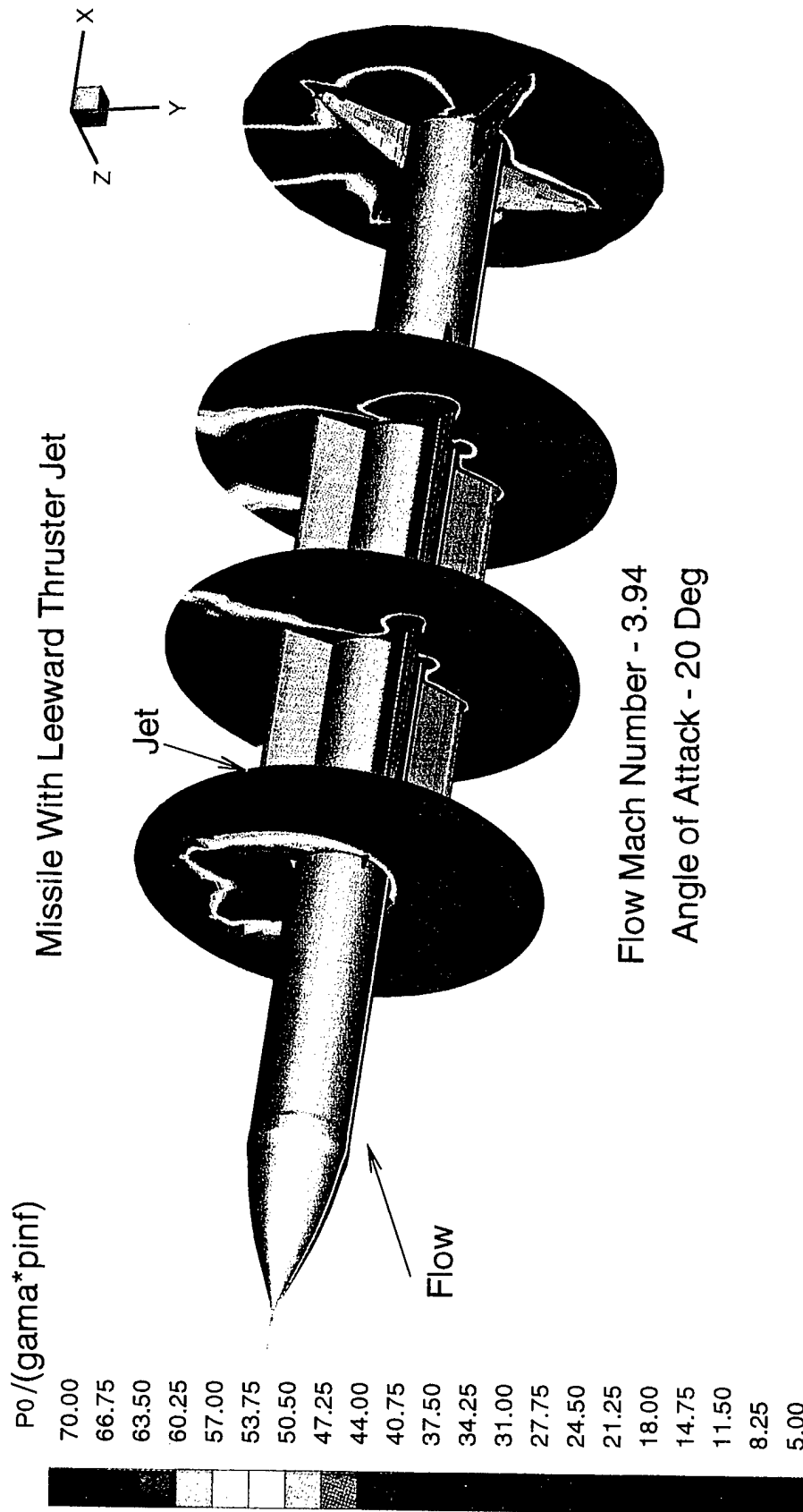
Fig. 11 - CFD Simulation of Wind Tunnel Geometry Without Jet



Pressure Distribution on Missile Surfaces Showing Leeward Jet Interaction Effects

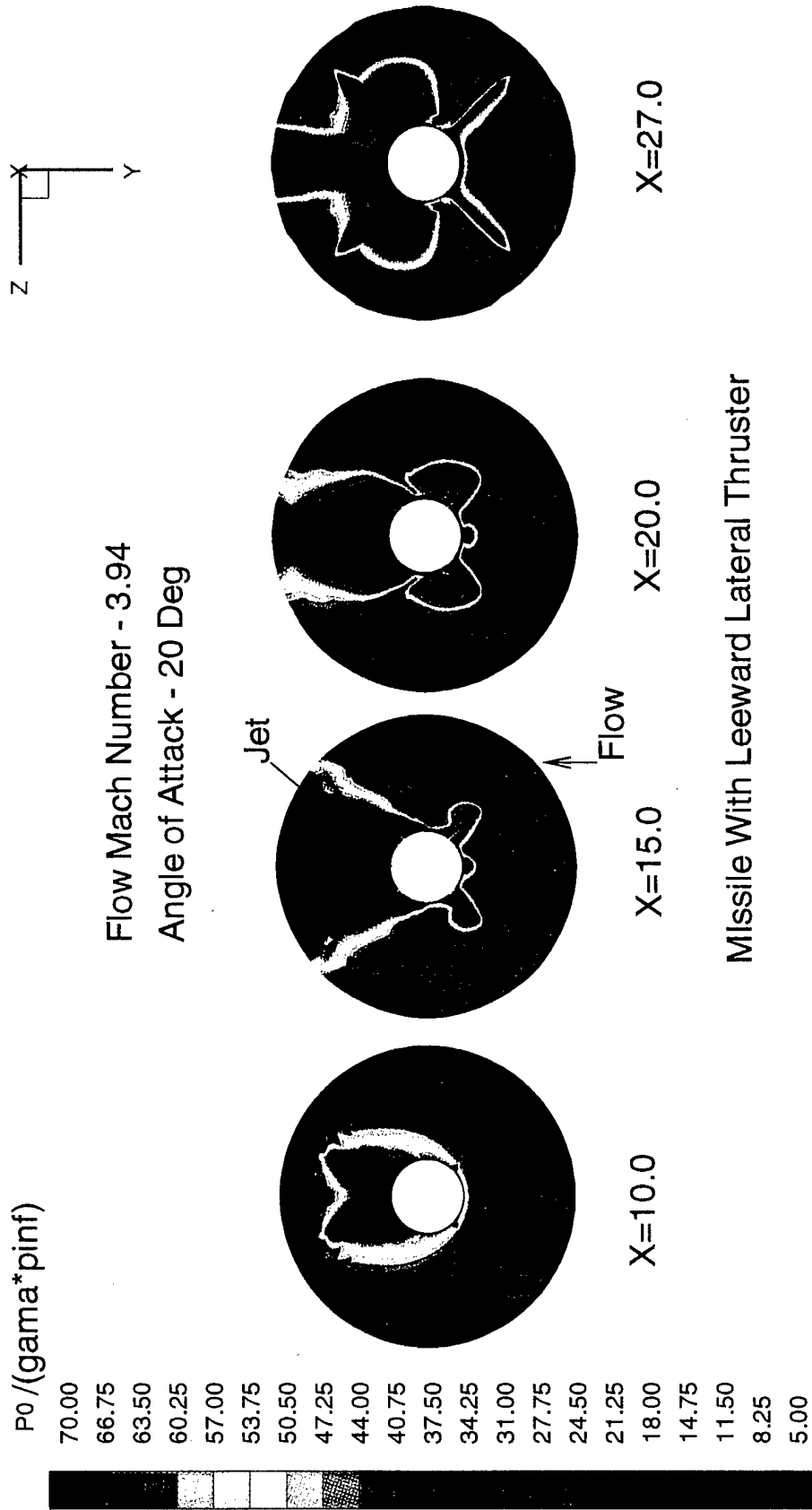
Fig. 12a - CFD Simulation of Wind Tunnel Geometry With Leeward Jet

UNCLASSIFIED



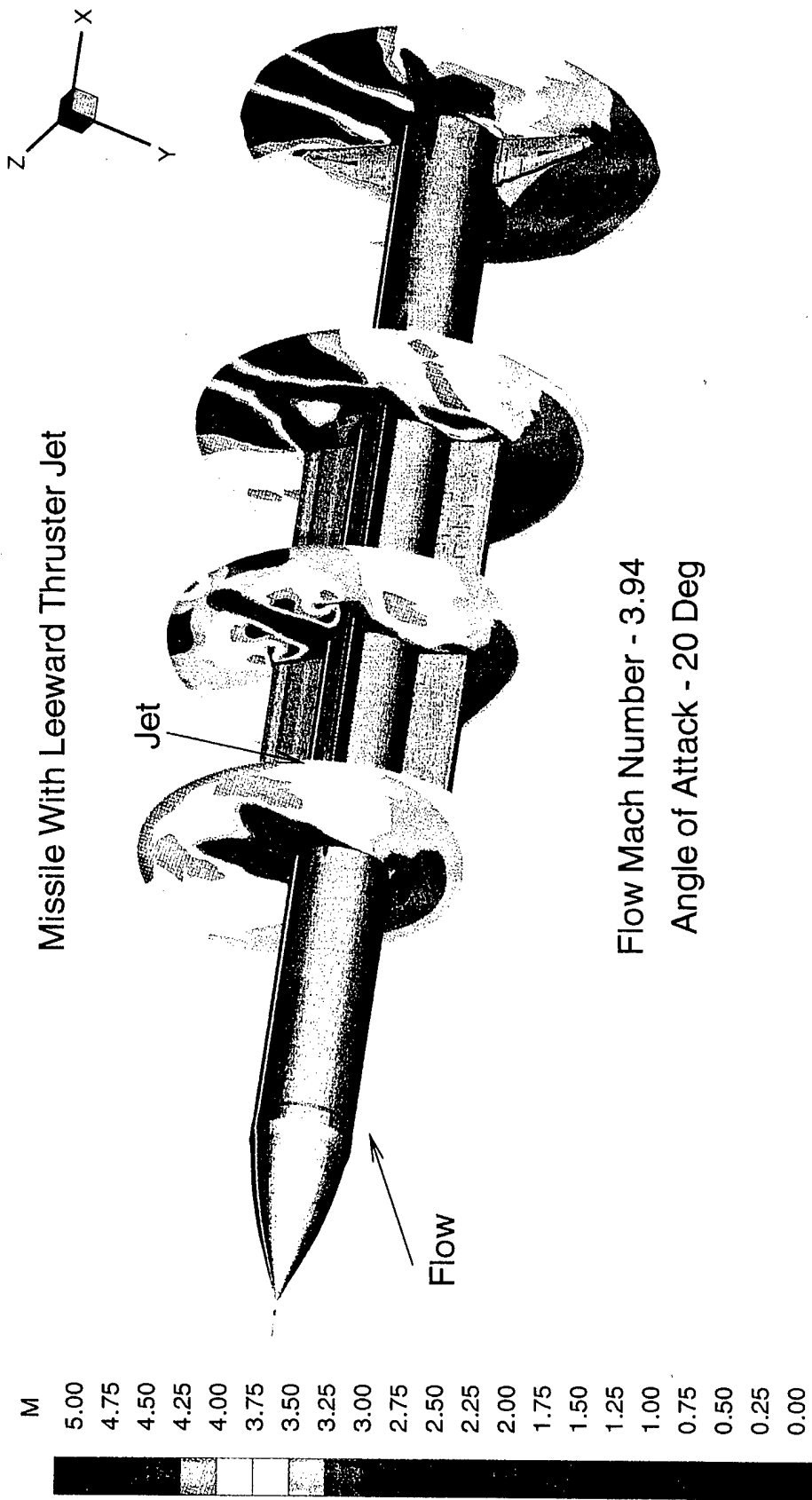
Total Pressure Contours at Several Axial Locations Showing Jet Effects

Fig. 12b - CFD Simulation of a Missile With Wings, Tail Panels and Lateral Thruster Jet



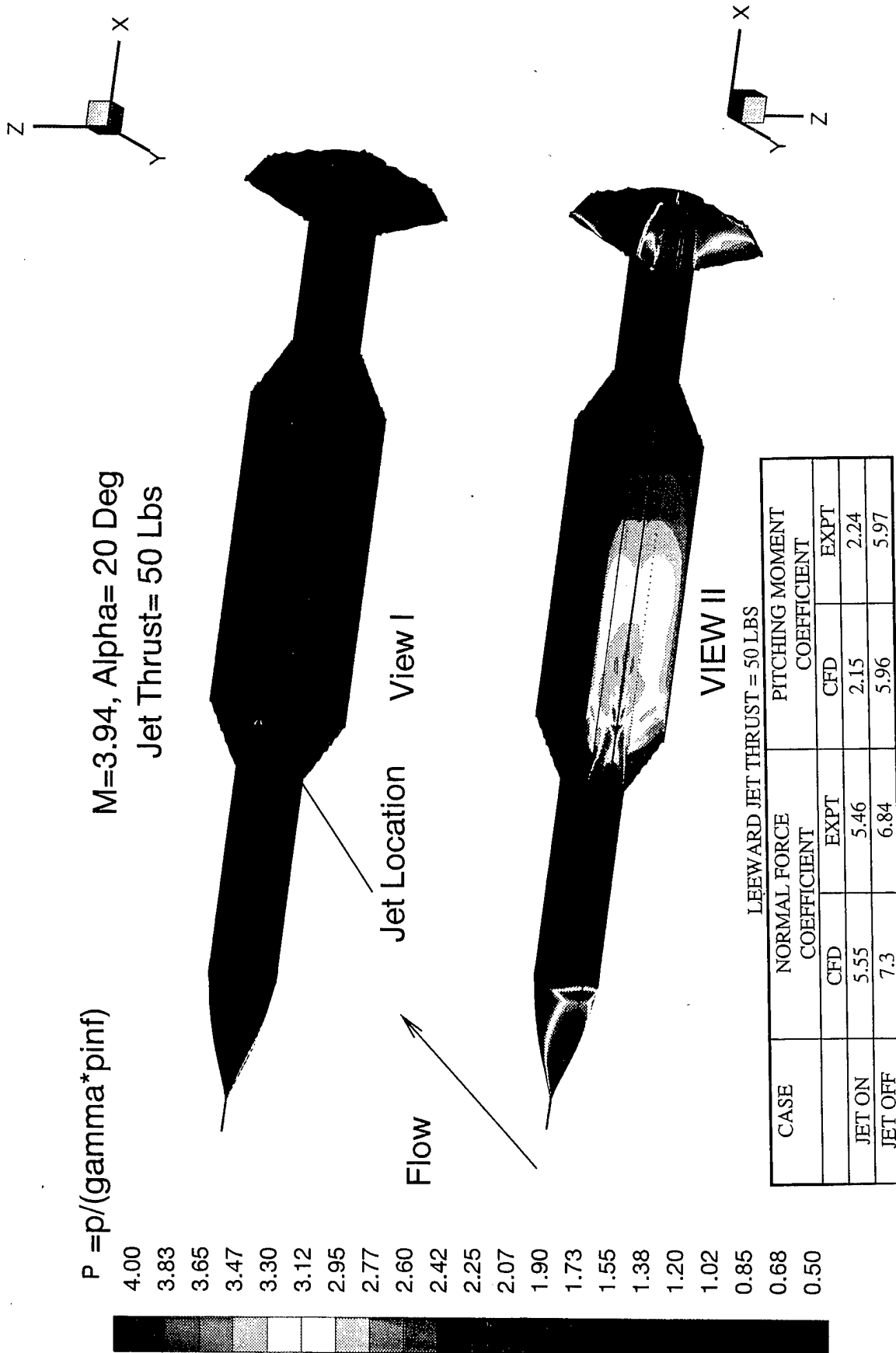
Total Pressure Contours at Various Axial Locations Showing Vortex Formation

Fig. 12c - Vortex Formation on a Missile With Wings, Tail Panels and Lateral Thruster



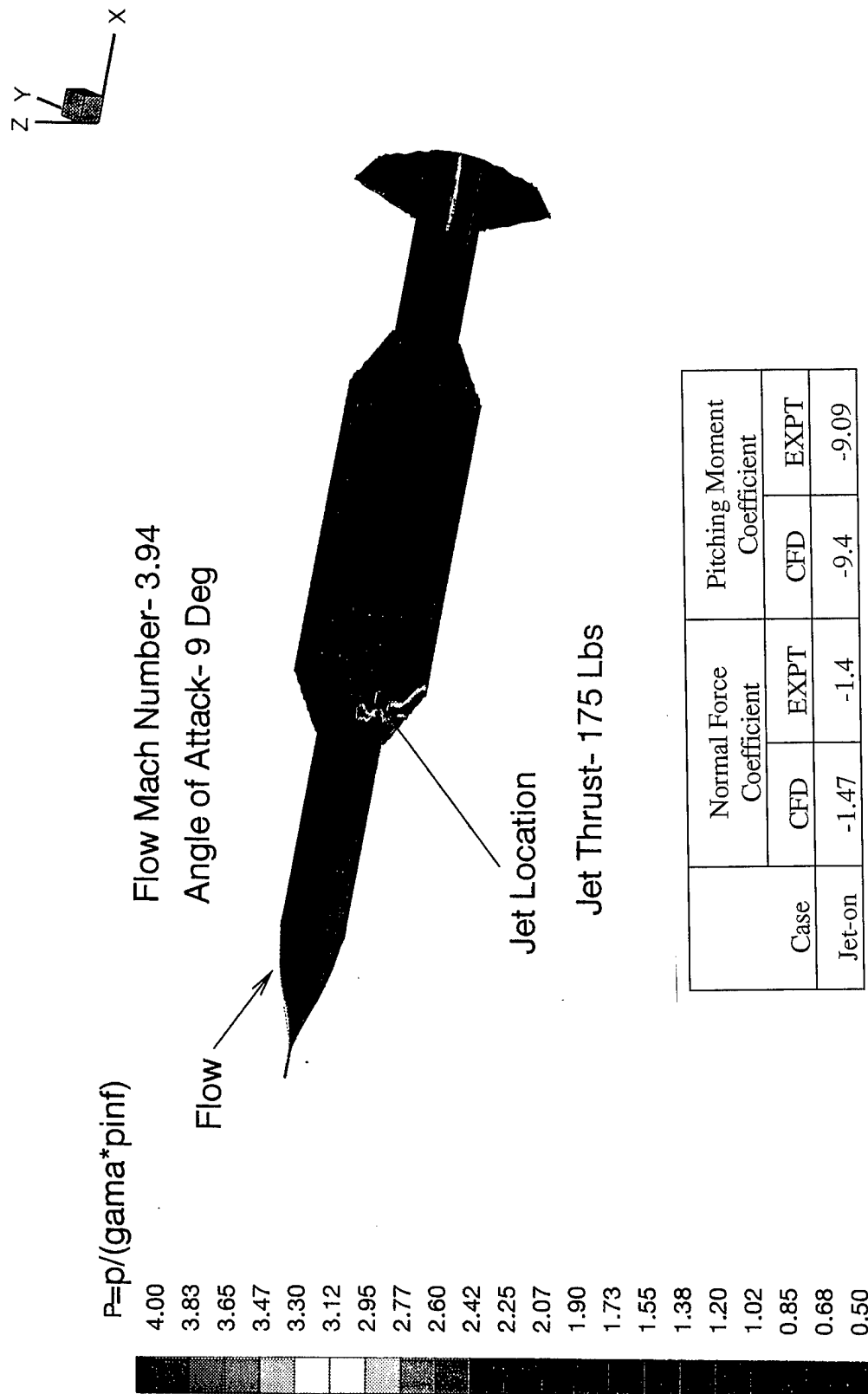
Mach Number Contours at Several Axial Locations Showing Jet Effects

Fig. 12d - CFD Simulation of a Missile With Wings, Tail Panels and Lateral Thruster Jet



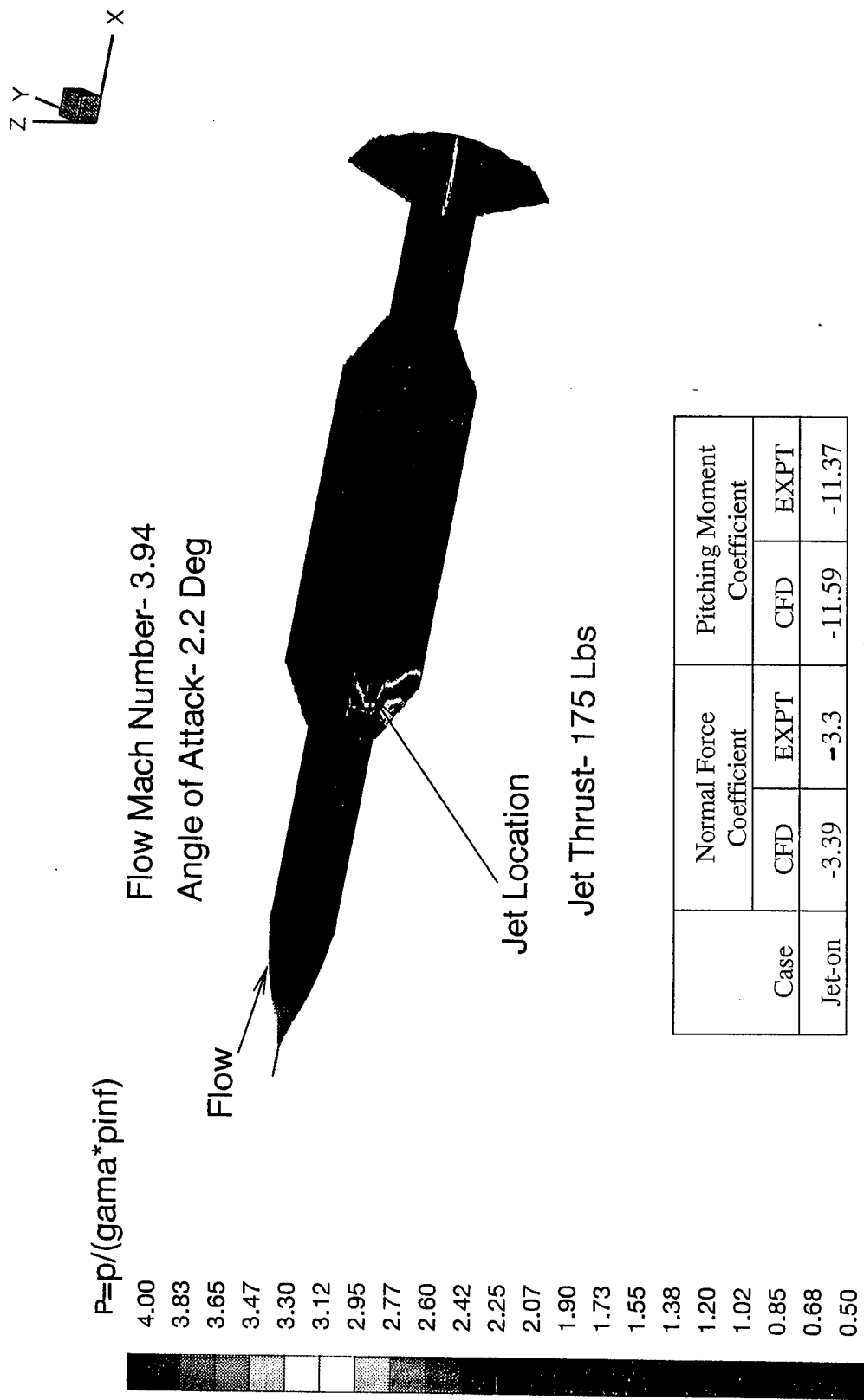
Pressure Distribution on Missile Surfaces With Leeward Jet Showing Jet Interaction Effects

Fig. 13 - CFD Simulation of Wind Tunnel Geometry With Leeward Jet



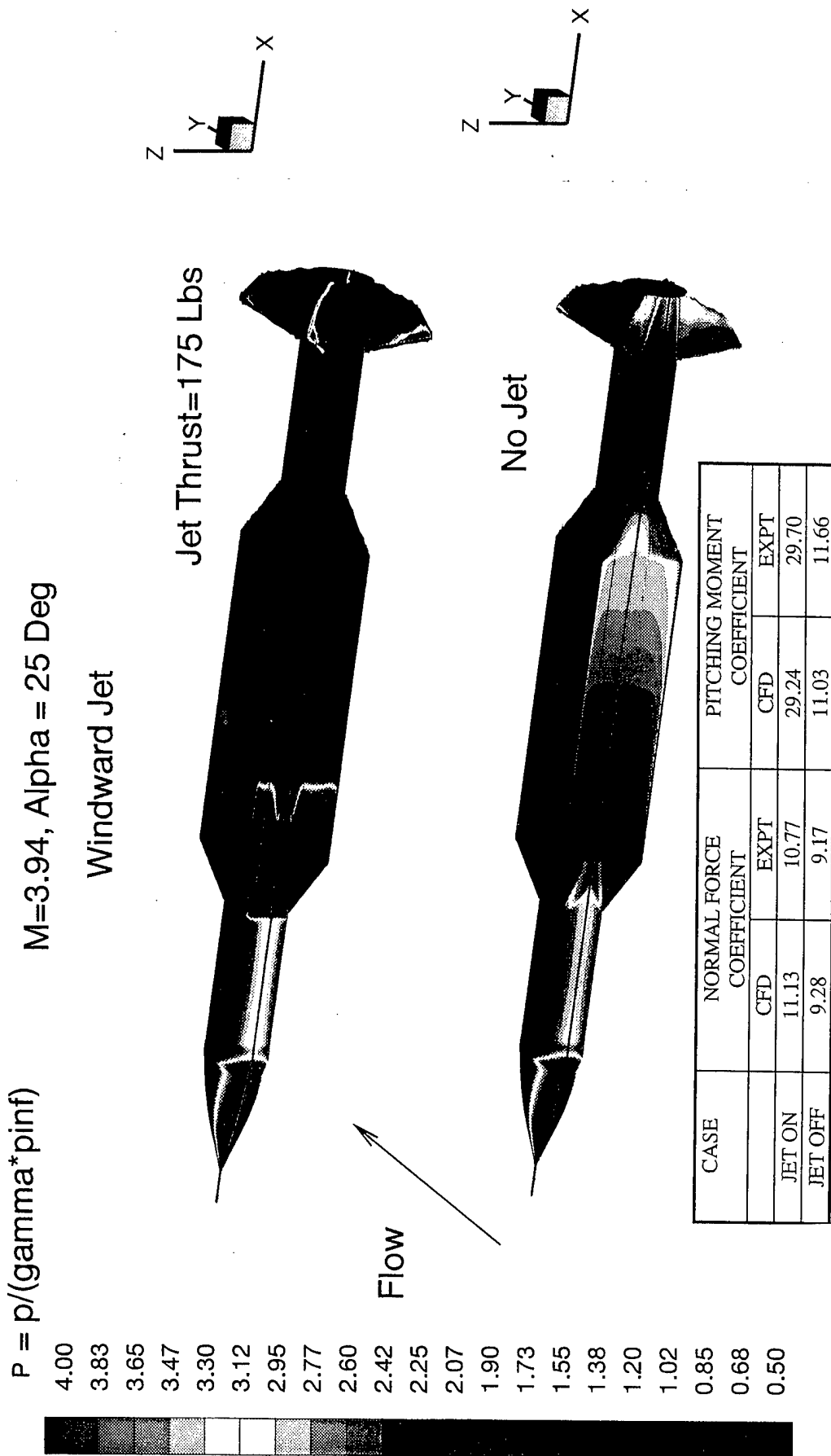
Missile Surface Pressure Distribution Showing Jet Interaction Effects

Fig. 14 - CFD Simulation of Wind Tunnel Geometry With Leeward Jet



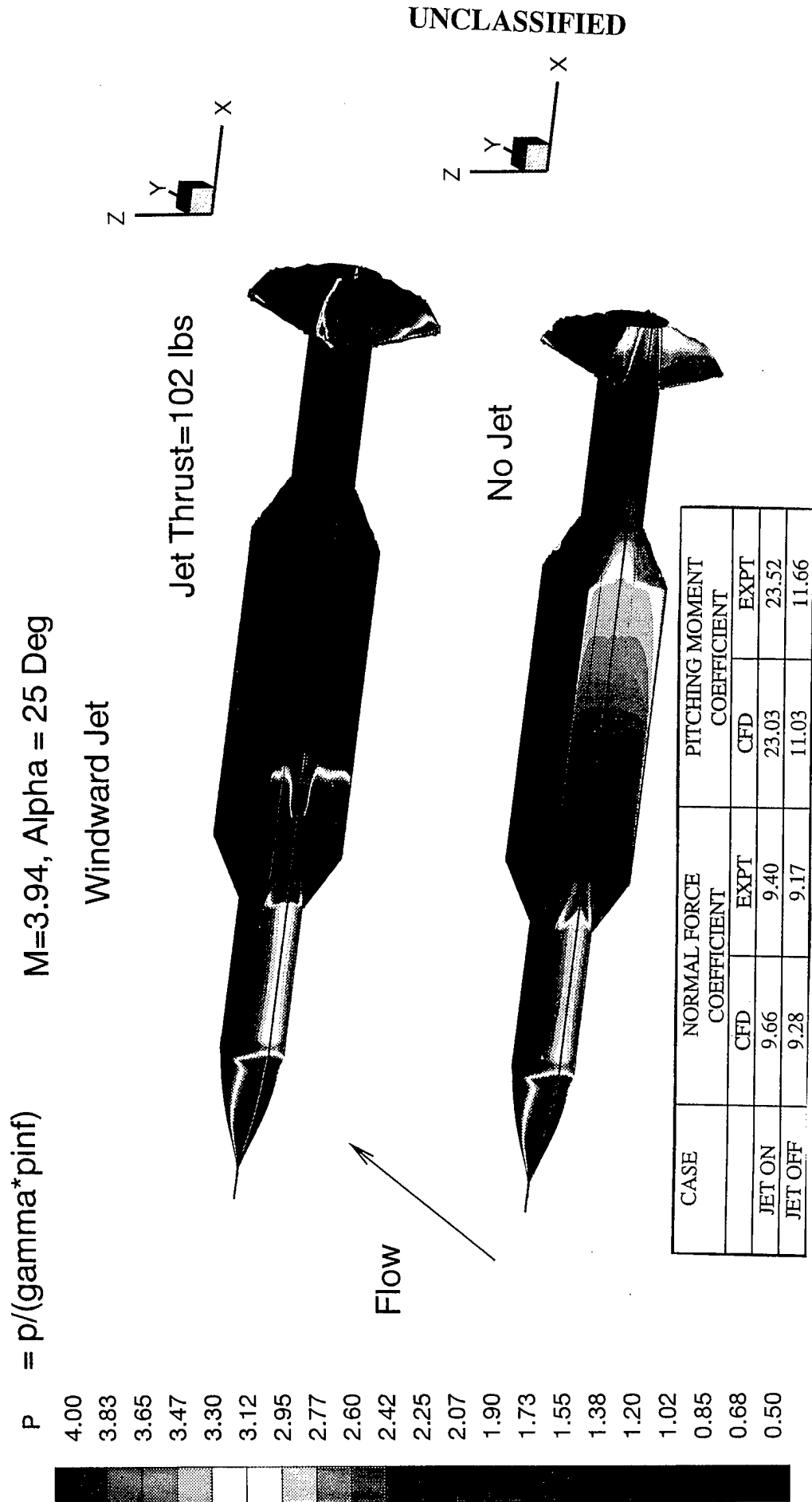
Missile Surface Pressure Distribution Showing Jet Interaction Effects

Fig. 15 - CFD Simulation of Wind Tunnel Geometry With Leeward Jet



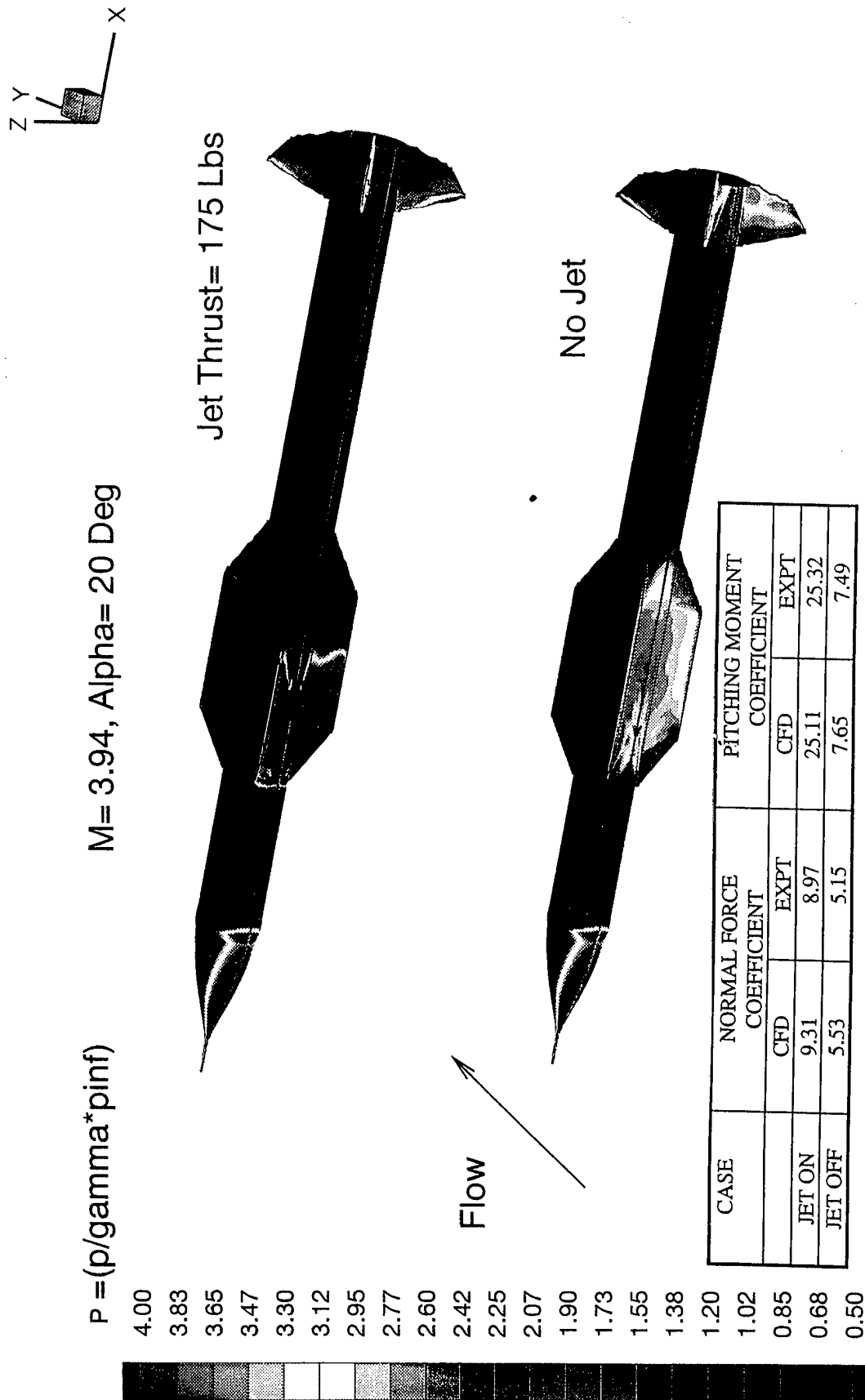
Pressure Distribution on Missile Surfaces Showing Jet Interaction Effects

Fig. 16 - CFD Simulation of Wind Tunnel Geometry With Forward Wings



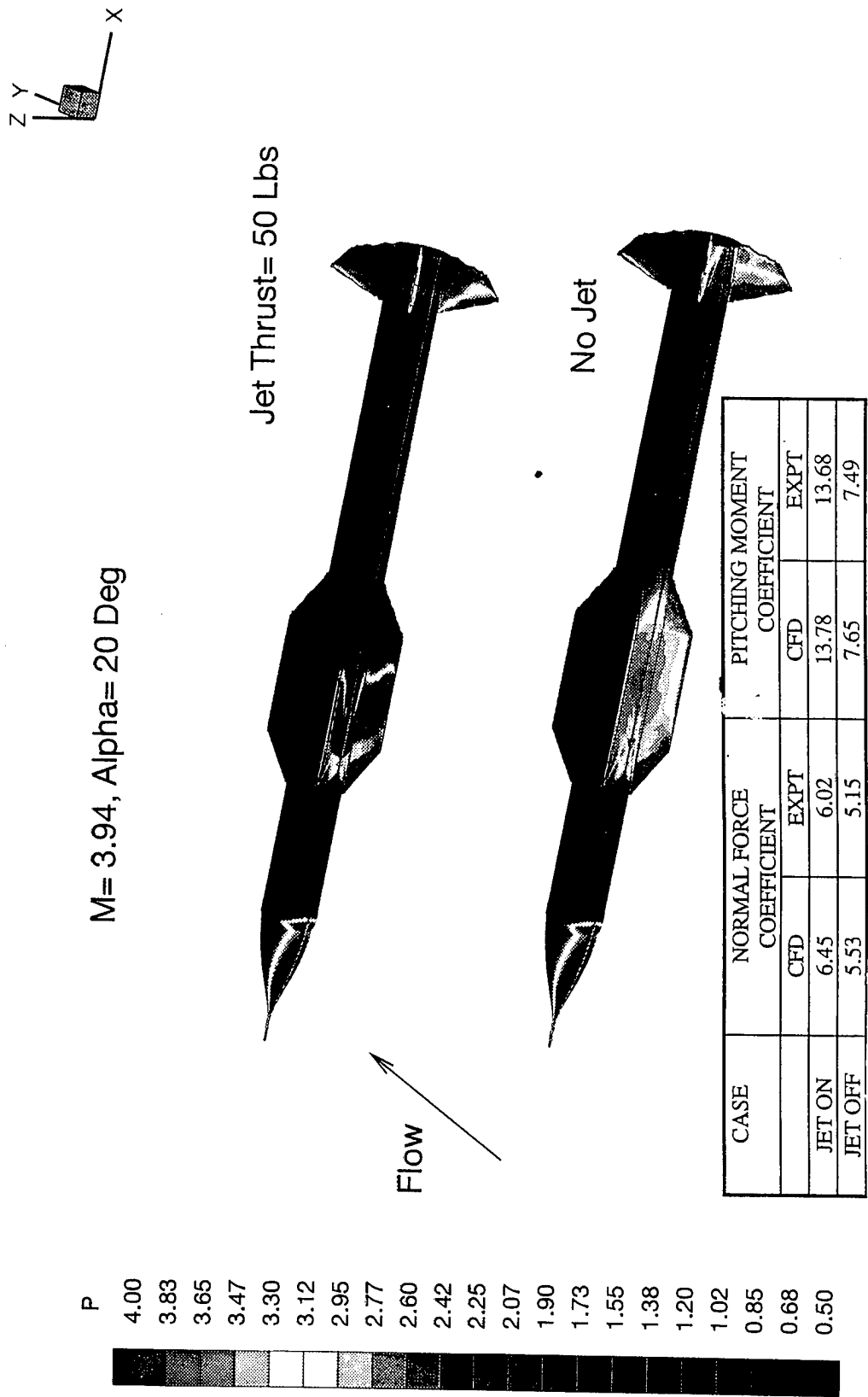
Pressure Distribution on Missile Surfaces Showing Jet Interaction Effects

Fig. 17 - CFD Simulation of Wind Tunnel Geometry With Forward Wings



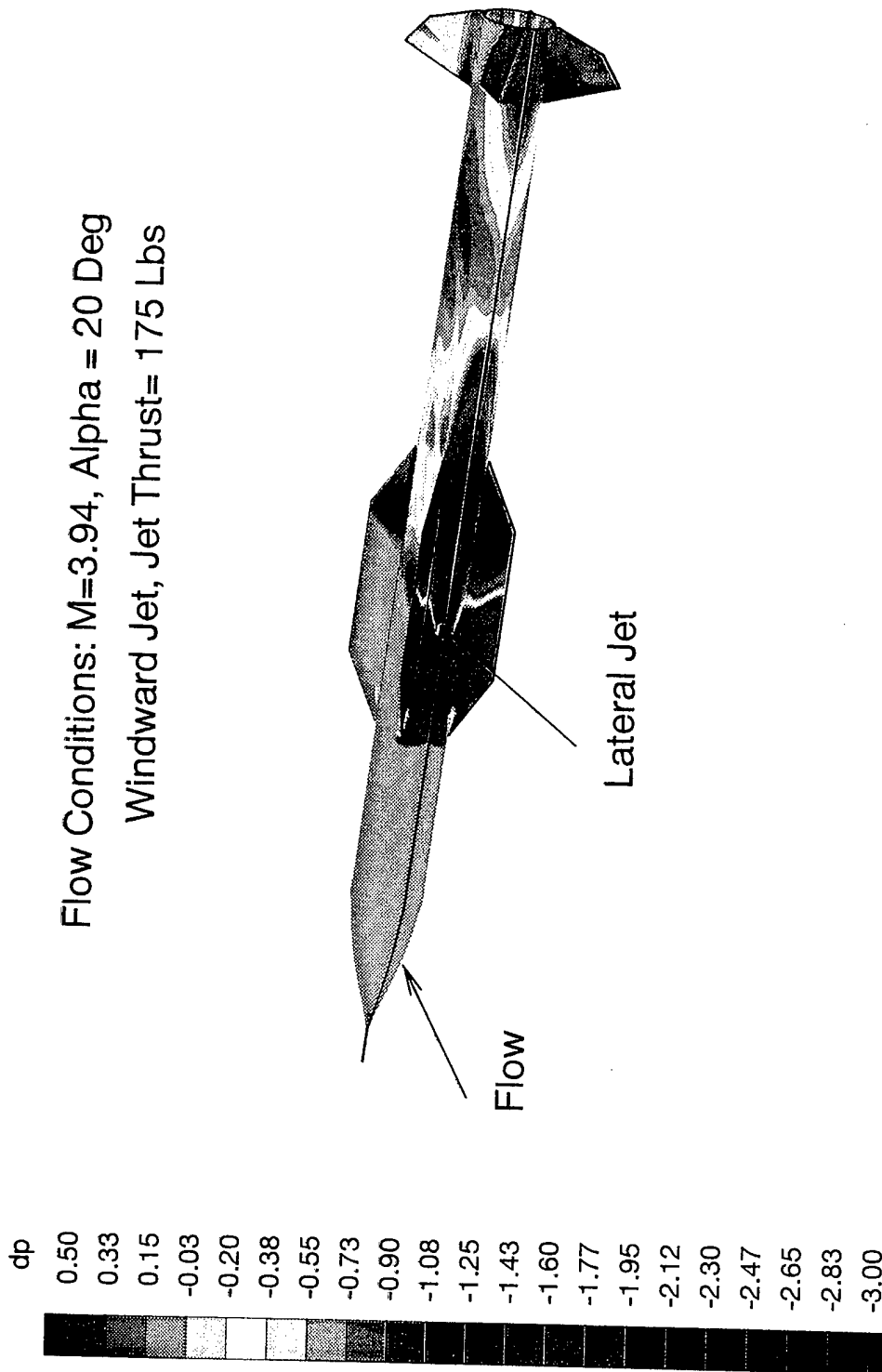
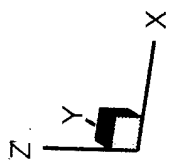
Pressure Distribution on Missile Surfaces Showing Jet Interaction Effects

Fig. 18 - CFD Simulation of Wind Tunnel Geometry With Short Wings



Pressure Distribution on Missile surfaces Showing Jet Interaction Effects

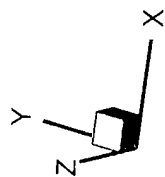
Fig. 19 - CFD Simulation of Wind Tunnel Geometry With Short Wings



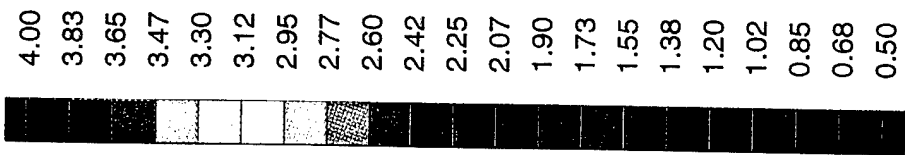
11-80

Surface Pressure Differential for Jet on and Jet off showing Jet Interaction Effects

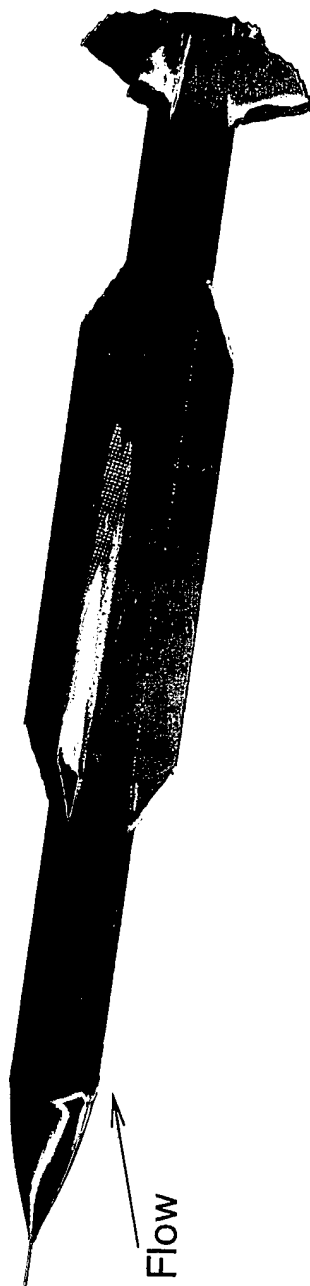
Fig. 20 - CFD Simulation of Wind Tunnel Geometry With Short Wings



$P / (\gamma \rho a^2)$



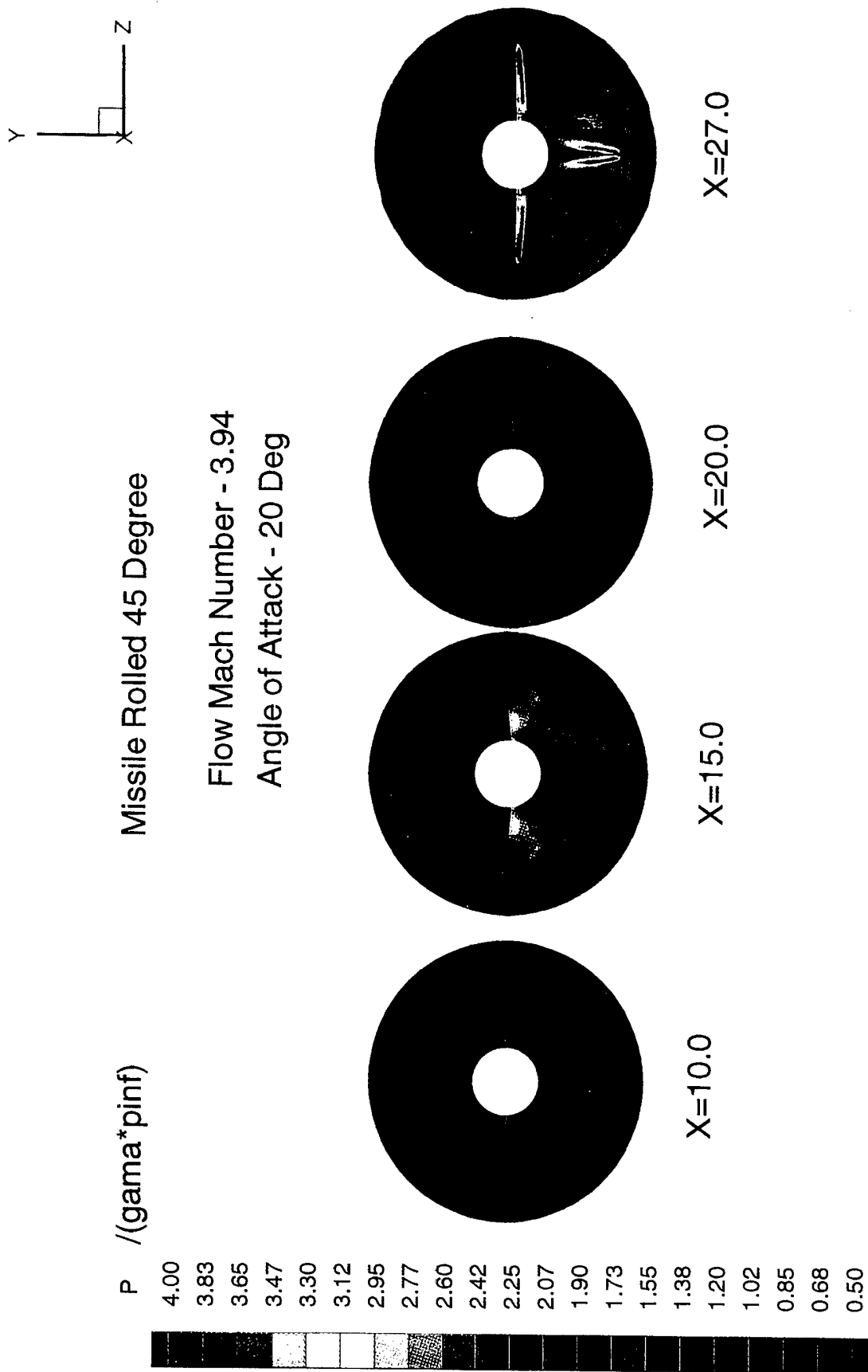
Flow Mach Number - 3.94
Angle of Attack - 20 Deg



Coefficient	CFD, alpha=20, phi=0	EXPT, alpha=19.8, phi=0.22
Force Coefficient	7.33	7.57
Moment Coefficient	3.89	2.57

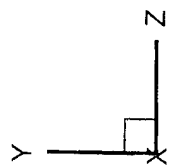
Missile Surface Pressure Distribution Showing Windward Surfaces

Fig. 21a - CFD Simulation of a Missile Without Lateral Jet

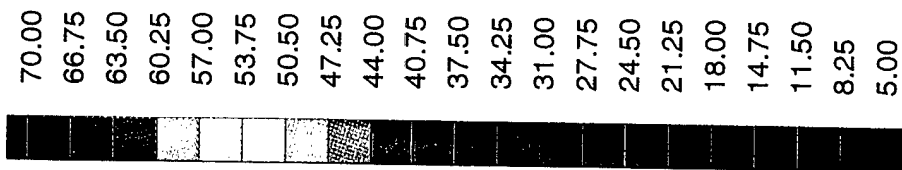


Pressure Distribution at Several Axial Locations for a Missile

Fig. 21b - CFD Simulation of a Missile Without Lateral Jet



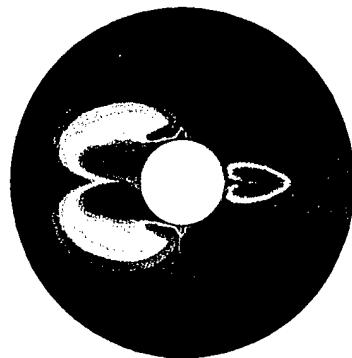
$P_0 / (\gamma \cdot p_{inf})$



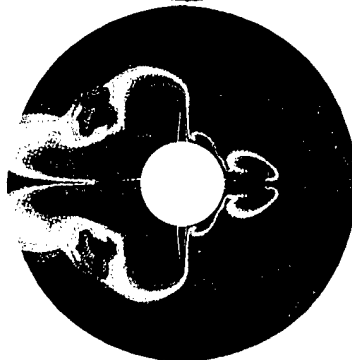
Missile Rolled 45 Degree

Flow Mach Number - 3.94

Angle of Attack - 20 Deg



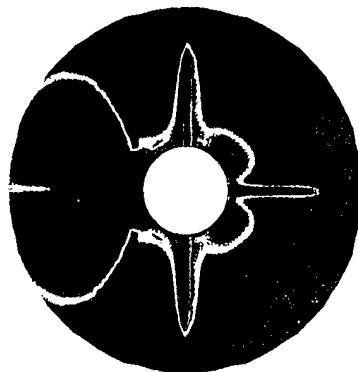
X=10.0



X=15.0



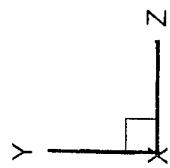
X=20.0



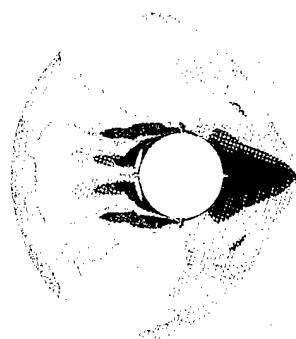
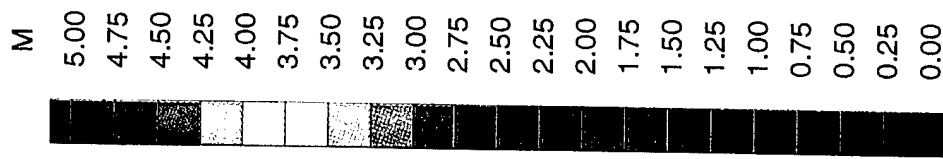
X=27.0

Total Pressure Distribution at Several Axial Locations for a Missile

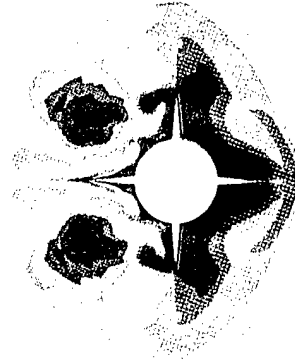
Fig. 21c - CFD Simulation of a Missile Without Lateral Jet



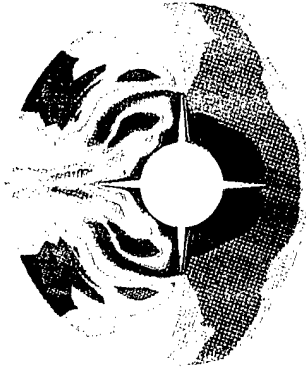
Missile Rolled 45 Degree
 Flow Mach Number - 3.94
 Angle of Attack - 20 Deg



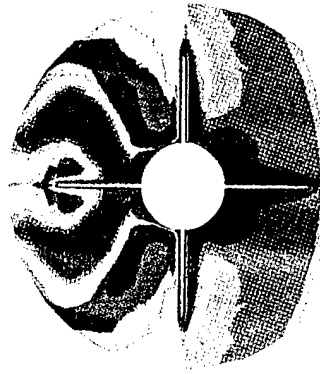
X=10.0



X=15.0



X=20.0



X=27.0

Mach Number Distribution at Several Axial Locations for a Missile

Fig. 21d - CFD Simulation of a Missile Without Lateral Jet

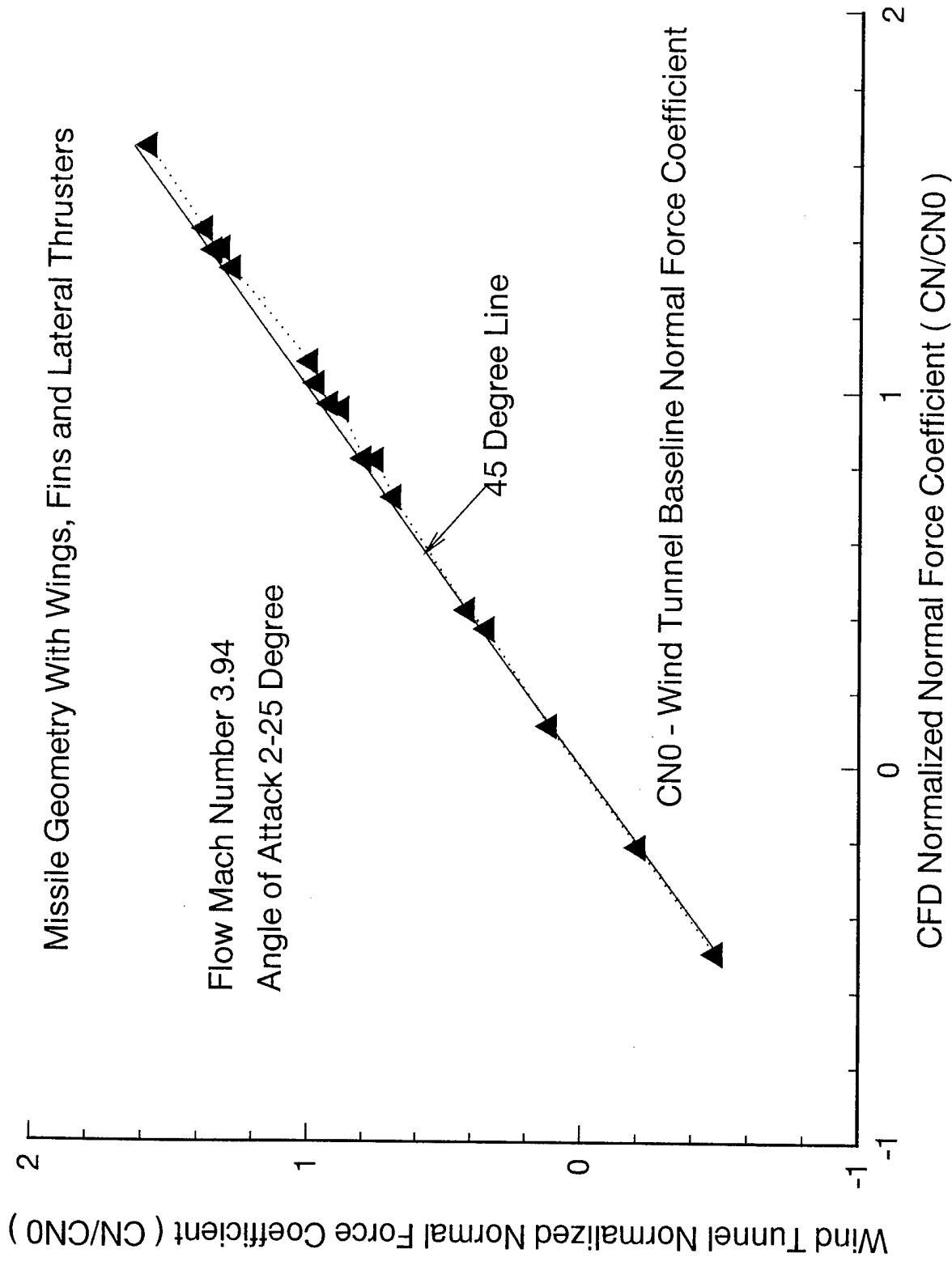


Fig. 22 - Comparison of CFD and Wind Tunnel Normalized Normal Force Coefficient

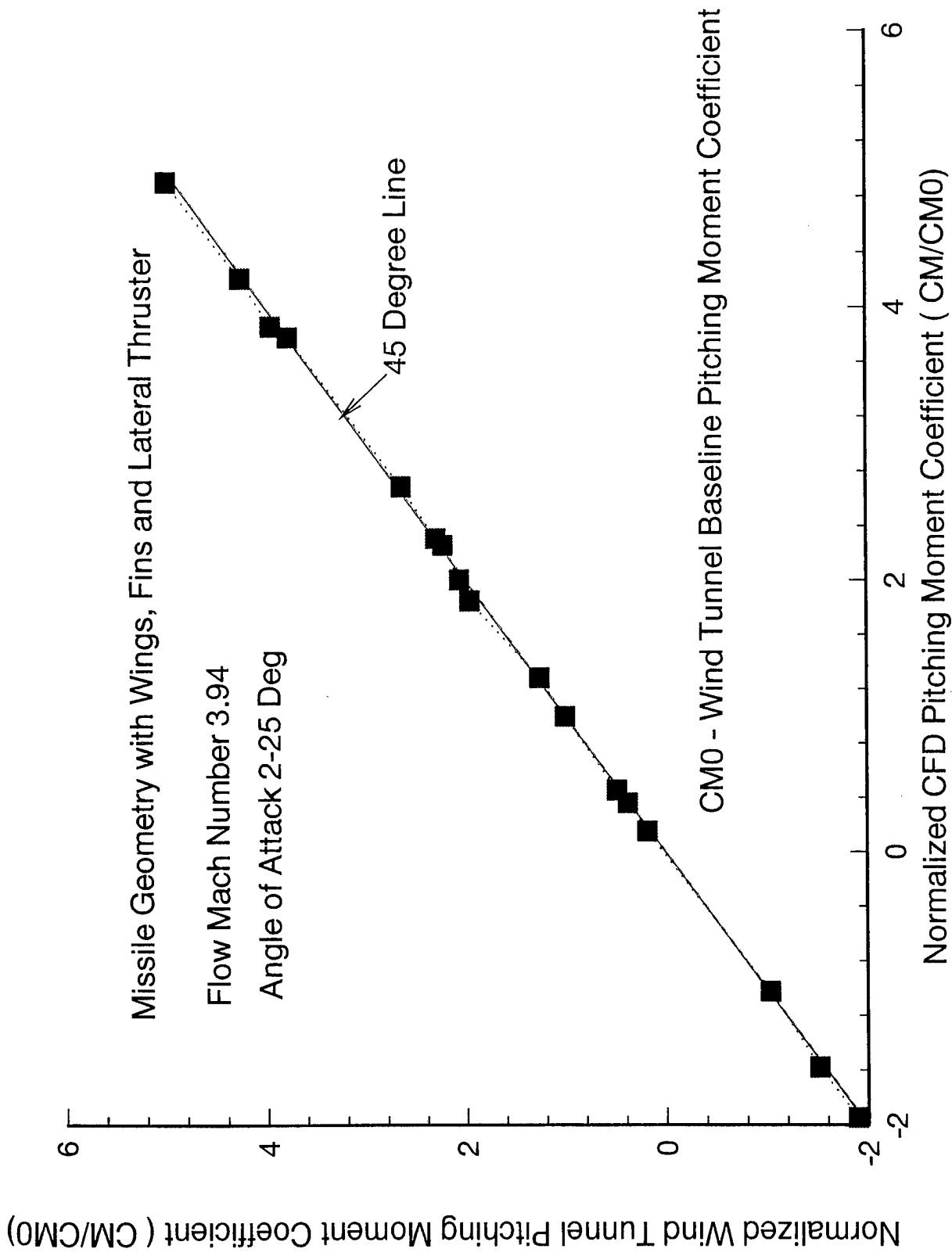


Fig. 23 - Comparison of CFD and Wind Tunnel Pitching Moment Coefficient